



HAL
open science

Linking Dynamic Water Storage and Subsurface Geochemical Structure Using High-Frequency Concentration-Discharge Records

Paul Floury, Julien Bouchez, Jennifer Druhan, Jérôme Gaillardet, Arnaud
Blanchouin, Éric Gayer, Patrick Ansart

► **To cite this version:**

Paul Floury, Julien Bouchez, Jennifer Druhan, Jérôme Gaillardet, Arnaud Blanchouin, et al.. Linking Dynamic Water Storage and Subsurface Geochemical Structure Using High-Frequency Concentration-Discharge Records. *Water Resources Research*, 2024, 60 (1), pp.e2022WR033999. 10.1029/2022WR033999 . hal-04404699

HAL Id: hal-04404699

<https://hal.inrae.fr/hal-04404699v1>

Submitted on 19 Jan 2024

HAL is a multi-disciplinary open access archive for the deposit and dissemination of scientific research documents, whether they are published or not. The documents may come from teaching and research institutions in France or abroad, or from public or private research centers.

L'archive ouverte pluridisciplinaire **HAL**, est destinée au dépôt et à la diffusion de documents scientifiques de niveau recherche, publiés ou non, émanant des établissements d'enseignement et de recherche français ou étrangers, des laboratoires publics ou privés.



Distributed under a Creative Commons Attribution 4.0 International License

Water Resources Research®



RESEARCH ARTICLE

10.1029/2022WR033999

Linking Dynamic Water Storage and Subsurface Geochemical Structure Using High-Frequency Concentration-Discharge Records

Paul Flourey¹ , Julien Bouchez^{1,2} , Jennifer L. Druhan^{1,2} , Jérôme Gaillardet¹ ,
Arnaud Blanchouin³ , Éric Gayer¹, and Patrick Ansart³

¹Institut de Physique du Globe de Paris, CNRS, Université Paris-Cité, Paris, France, ²Department of Earth Science & Environmental Change, University of Illinois Urbana Champaign, Urbana, IL, USA, ³ORACLE, Institut National de Recherche pour l'Agriculture, l'Alimentation et l'Environnement, Antony, France

Key Points:

- We combine high-frequency (every 40 min) stream chemistry data and stream discharge recession analysis
- We propose a conceptual model for the relationship between water storage and solute export at the Orgeval Critical Zone Observatory (CZO), France
- Three classes of solute behavior are identified at the Orgeval CZO, related to the role of rock dissolution and amendments in their budget

Supporting Information:

Supporting Information may be found in the online version of this article.

Correspondence to:

J. Bouchez,
bouchez@ipgp.fr

Citation:

Flourey, P., Bouchez, J., Druhan, J. L., Gaillardet, J., Blanchouin, A., Gayer, É., & Ansart, P. (2024). Linking dynamic water storage and subsurface geochemical structure using high-frequency concentration-discharge records. *Water Resources Research*, 60, e2022WR033999. <https://doi.org/10.1029/2022WR033999>

Received 15 NOV 2022
Accepted 30 NOV 2023

Author Contributions:

Conceptualization: Paul Flourey, Julien Bouchez, Jennifer L. Druhan, Jérôme Gaillardet

Data curation: Paul Flourey, Julien Bouchez, Jérôme Gaillardet, Arnaud Blanchouin, Patrick Ansart

Formal analysis: Paul Flourey, Julien Bouchez, Jennifer L. Druhan, Éric Gayer

Funding acquisition: Jérôme Gaillardet

Investigation: Paul Flourey, Julien Bouchez, Jennifer L. Druhan, Jérôme Gaillardet, Éric Gayer

Abstract Shifts in water fluxes and chemical heterogeneity through catchments combine to dictate stream solute export from the Critical Zone. The ways in which these factors emerge in resultant concentration-discharge ($C-Q$) relationships remain obscure, particularly at the timescale of individual precipitation and discharge events. Here we take advantage of a new high-frequency, multi-element and multi-event stream $C-Q$ data set. The stream solute concentrations of seven major ions were recorded every 40 min over five flood events spanning one hydrologic year in a French agricultural watershed (Orgeval) using a lab-in-the-field deployment we refer to as a “River Lab.” We focus attention on the recession periods of these events to consider how geochemical heterogeneity within the catchment translates into dynamic stream solute concentrations during shifts in water storage. We first show that for $C-Q$ relationships resulting from data acquisition over multiple flood events, lumping all trends together can lead to biases in characteristic $C-Q$ parameters. We then reframe $C-Q$ relationships using a simple recession curve analysis to consider how hydrological processes produce chemical mixing of distinct solute pools immediately following discharge events. We find three distinct classes of behavior among the major solutes, none of which can be interpreted based on water storage changes alone. The shape of $C-Q$ relationships for each solute can then be related to their vertical zonation in the subsurface of Orgeval, and to the capacity for subcomponents of these distributions to be readily mobilized during a discharge event.

1. Introduction

The storage and movement of water through landscapes exerts a fundamental control on solute export from catchments (Berner, 1978; Godsey et al., 2019; Kolbe et al., 2019; Maher, 2010, 2011; Marçais et al., 2015; Stewart et al., 2022; Torres et al., 2015; Wolock et al., 1997). Stream solute concentration - discharge ($C-Q$) relationships have been widely utilized to study catchment-scale linkages between hydrodynamics and hydrochemistry (e.g., House & Warwick, 1998; Knapp et al., 2022; Musolff et al., 2015; Pinder & Jones, 1969; White & Blum, 1995). Existing data records span a broad range of temporal scales, from multi-annual, relatively low-frequency monitoring (typically daily to weekly; Basu et al., 2010, 2011; Godsey et al., 2009; ; Ibarra et al., 2016; Knapp et al., 2022; McIntosh et al., 2017; Musolff et al., 2015; Stewart et al., 2022; Wymore et al., 2017) to event-scale, high-frequency (typically better than daily) observations (Godsey et al., 2019; Herndon et al., 2015; Knapp et al., 2020; Rose et al., 2018; Winnick et al., 2017; Wymore et al., 2019). Across such a diversity of timescales, a fundamental observation has emerged, that $C-Q$ patterns change depending on the time scale and resolution of the data record (Duncan et al., 2017; Dupas et al., 2017; Fazekas et al., 2020; Godsey et al., 2019; Knapp et al., 2020; Li, 2019; Zhi et al., 2019).

$C-Q$ patterns tracked at relatively coarse frequencies have commonly been interpreted as the signatures of watershed “reactors” responding to shifts in the balance between timescales of water fluxes and chemical reaction kinetics (Clow & Mast, 2010; Godsey et al., 2009, 2019; Ibarra et al., 2016; Langbein & Dawdy, 1964; Maher, 2011; Maher & Chamberlain, 2014; Maher & Druhan, 2014; Torres et al., 2015; Wymore et al., 2017). In contrast, and given the brevity of most individual precipitation events in small catchments, seasonal to event-scale $C-Q$ relationships have largely been attributed to the effect of transient mixtures of multiple water and solute pools already existing in the catchment before discharge increases (e.g., Basu et al., 2010, 2011; Bouchez et al., 2017; Calmels et al., 2011; Chanut et al., 2002; Evans & Davies, 1998; Johnson et al., 1969; Kim

© 2024. The Authors.

This is an open access article under the terms of the [Creative Commons Attribution License](https://creativecommons.org/licenses/by/4.0/), which permits use, distribution and reproduction in any medium, provided the original work is properly cited.

Methodology: Paul Flourey, Julien Bouchez, Jennifer L. Druhan, Jérôme Gaillardet, Arnaud Blanchouin, Éric Gayer, Patrick Ansart

Project Administration: Jérôme Gaillardet

Resources: Jérôme Gaillardet, Arnaud Blanchouin, Patrick Ansart

Software: Paul Flourey, Julien Bouchez, Jennifer L. Druhan, Arnaud Blanchouin, Éric Gayer

Supervision: Julien Bouchez, Jennifer L. Druhan, Jérôme Gaillardet

Validation: Paul Flourey, Julien Bouchez, Jennifer L. Druhan, Arnaud Blanchouin, Patrick Ansart

Visualization: Paul Flourey, Julien Bouchez, Jennifer L. Druhan, Éric Gayer

Writing – original draft: Paul Flourey, Julien Bouchez, Jennifer L. Druhan, Jérôme Gaillardet, Arnaud Blanchouin, Éric Gayer

Writing – review & editing: Paul Flourey, Julien Bouchez, Jennifer L. Druhan, Jérôme Gaillardet, Arnaud Blanchouin, Éric Gayer

et al., 2017; Knapp et al., 2022; Musolff et al., 2015; Rose et al., 2018; Rue et al., 2017; Seibert et al., 2009; Vaughan et al., 2017; Wymore et al., 2019). Such pre-existing solute pools might be conceptualized as water pockets present in the basin but loosely connected to the stream before the event starts; or as readily exchangeable species present on organic or mineral surfaces within the basin (e.g., Clow & Mast, 2010; Godsey et al., 2019). The mobilization of these solutes and their ability to contribute to stream export then depends on how infiltrating rainwater can “wet” the parts of the catchments where solutes are stored, which might in turn depend on antecedent conditions and the characteristics of each individual discharge event (Knapp et al., 2022; Seibert et al., 2009; Thompson et al., 2011). A variety of intermediary interpretations have also been proposed, combining multiple water pools and pathways, each uniquely characterized by their own water-rock reactivity (e.g., Druhan & Maher, 2017; Hornberger et al., 2001; Moatar et al., 2017; Stewart et al., 2022; Winnick et al., 2017).

Interpretation of event-scale $C-Q$ patterns as a reflection of mixing and (re)routing of geochemically distinct water pools in the near-surface has two major implications. First, it requires that near-surface environments are not geochemically homogeneous, and second, that stream solutes are sensitive to shifts in the export of water stored in these geochemically distinct pools during and following infiltration events. Geochemical heterogeneity of the near-surface leading to zonation of dissolved solutes has been extensively described. Early examples include seasonal activation of flow through shallow, organic-rich soils driving export of dissolved organic carbon (DOC) from upland watersheds (Boyer et al., 1996; Hornberger et al., 1994; Mei et al., 2012, 2014). $C-Q$ patterns over a variety of elements, timescales and sampling resolutions have subsequently been interpreted as a result of catchment geochemical heterogeneity (e.g., Baronas et al., 2017; Bouchez et al., 2017; Herndon et al., 2015; Torres et al., 2017; Xiao et al., 2021). For example, observations taken from instrumented field sites support models of nested pyrite and carbonate weathering fronts (Brantley et al., 2013; Sullivan et al., 2016), which have been subsequently invoked to explain $C-Q$ hysteresis in other shale lithologies (Winnick et al., 2017). Numerical reactive transport models of $C-Q$ patterns have required the description of specific mineral distributions and ecosystem functions to explain differences among multiple elements (Zhi et al., 2019). These inferences have led to a recent renewal of “shallow and deep” hypotheses to explain nitrate $C-Q$ patterns across 228 watersheds at coarse sampling frequency (Zhi & Li, 2020); as well as several years of multi-element $C-Q$ patterns across two watersheds (Stewart et al., 2022). A similar conceptualization of lateral hydrologic connectivity driving solute mobilization between different areas of a catchment was recently used to describe multi-element $C-Q$ patterns at coarse frequency across four watersheds (Knapp et al., 2022).

These examples (e.g., nested weathering fronts, shallow and deep hypothesis, lateral connectivity) collectively illustrate a foundation of $C-Q$ pattern interpretation based on catchment geochemical heterogeneity. However, most of the $C-Q$ data reported in these studies still reflect relatively coarse observational frequencies for hydrochemistry in comparison to discharge and precipitation records. Hydrologic models for individual infiltration and discharge events date back to the early recognition that a hydrograph can be split into the contribution of multiple sources (Pinder & Jones, 1969; Sklash & Farvolden, 1979), often described as a variety of fast and slow pathways, or young and old pools. Early assumptions of linear, static runoff response to infiltration events were replaced by non-linear relationships between discharge and subsurface storage through recession curve analysis (Brutsaert & Nieber, 1977; Kirchner, 2009; Nathan & McMahon, 1990; Wittenberg, 1999). These methods, in turn, have been recently adapted into StorAge Selection (SAS)-type models, which utilize tracer constraints to map transient functional relationships between the age of water stored in a catchment and the age of water discharging to streamflow during storm events (Benettin et al., 2022; Benettin, Soulsby, et al., 2017; Botter et al., 2011; Harman, 2015; Remondi et al., 2018; Rinaldo et al., 2015). Basic relationships between water age and the evolution of kinetically-controlled solute chemistry have been shown to produce reasonable event-scale $C-Q$ patterns based on SAS-type hydrological models (Benettin, Bailey, et al., 2017), yet fundamental challenges remain in attempting to relate solute storage and stream export to runoff response.

The complexity inherent in identifying relationships between water storage variation and solute mobilization during hydrological events is demonstrated by considering a species-specific pool N (mol), corresponding to the mass of a given solute stored within the catchment which can be “mobilized” upon input of new water by precipitation. If we consider a single homogeneous storage volume S , then:

$$N = SC_S \quad (1)$$

where C_s describes the average concentration of the species in the storage volume. Similarly, we may define a solute mass flux out of the catchment, F (mol/s):

$$F = QC_Q \quad (2)$$

based on discharge (Q) and the concentration of the species in stream discharge (C_Q). A basic water balance relates the change in S to the difference between influxes (precipitation) and effluxes (evapotranspiration and discharge). Over the recession period of a hydrograph, this relationship may be simplified to the equivalency $\frac{dS}{dt} = -Q$ (Brutsaert & Nieber, 1977; Kirchner, 2009; Krier et al., 2012; Shaw & Riha, 2012). If we consider that source/sink terms such as mineral dissolution and precipitation do not influence C_s and C_Q over the timescale of a precipitation event, and similarly that atmospheric inputs are negligible during the recession period, then it follows that:

$$\frac{dN}{dt} = -F \quad (3)$$

Inserting Equations 1 and 2 into this expression and expanding yields:

$$\frac{dSC_s}{dt} = S\frac{dC_s}{dt} + C_s\frac{dS}{dt} = -F = -QC_Q$$

which simplifies to:

$$S\frac{dC_s}{dt} - QC_s = -QC_Q \quad (4)$$

in the recession period. Equation 4 illustrates the troubling circumstance that if $C_s = C_Q$ then $\frac{dC_s}{dt} = 0$ and thus there is no capacity for C_Q to vary during recession. Hence, the capacity of a single storage reservoir to plausibly produce variations in C_s for geogenic solutes over timescales of hydrologic events is extremely limited (Hall, 1970, 1971). Clearly, mixing between distinct solute pools within S is necessary to satisfy the ubiquitous observation of variable C_Q over the falling limb of storm hydrographs. Therefore a reasonable interpretation consistent with prior studies is that the fluid volume(s) dictating the mass(es) of stored solute(s) are not equivalent to S but rather some subset of stored water with specific chemical composition. The implication is that C_s must be heterogeneously distributed within the storage and could evolve independently from S , even if the dynamics of these two variables are in fact closely linked.

To date, a generalized and parsimonious approach to event-scale C - Q and storm hydrograph analysis remains to be established. Recent technological advances now offer the possibility for advancement through tracking of C - Q relationships for a large variety of elements at high frequency and over long timescales through deployment of “lab-in-the-field” devices (Floury et al., 2017; Rode et al., 2016; von Freyberg et al., 2017; Wang et al., 2024). Here we rely on such a device, called the “River Lab” (RL), to measure the full suite of stream major dissolved species at a sub-hourly frequency (Floury et al., 2017). This instrument allows us to explore C - Q relationships within and among five individual discharge events spread across the 2015–2016 hydrological year in the Orgeval Critical Zone Observatory (CZO), France, which is underlain by a layered aquifer system and characterized by agricultural land use. Our record of hydrological events spans over an order of magnitude in peak discharge and covers a diversity of antecedent hydroclimatic conditions including dry and wet seasons.

With the fine detail afforded by the RL data set, we seek to test the following hypothesis: variations in stream solute export over a hydrological event reflect the extent to which geochemical zonation of the catchment is accessed by dynamic water storage. Our first objective is to constrain relationships between S and Q , allowing us to recast our high frequency C - Q records as C versus S over the recession limb of each event. Our second objective is to identify conditions where a simple relationship between dynamic S and dynamic C is complicated by additional factors. Under these conditions, we consider distinctions in the pace and extent to which individual solutes return to pre-event conditions, to parse nuances in the geochemical structure of the watershed. Ultimately, this multi-element high-frequency data record allows us to describe C - Q relationships resulting from dynamic changes in water storage, and how these relationships are produced by chemically heterogeneous watershed structure (Ackerer et al., 2020; Basu et al., 2010; Bieroza et al., 2018; Moatar et al., 2017; Musolff et al., 2015; Pohle et al., 2021; Speir et al., 2021; Sullivan et al., 2019).

2. Study Area

The Orgeval CZO is an instrumented catchment located within the Seine watershed, situated 70 km to the east of Paris, France. This catchment is part of the French national Research Infrastructure OZCAR (Observatoire de la Zone Critique: Applications et Recherche; Gaillardet et al., 2018). Nutrient cycling (Garnier et al., 2014, 2016; Vilain et al., 2010, 2012), soil moisture (Carreau et al., 2009; Lauzon et al., 2004; Zribi & Dechambre, 2003; Zribi et al., 2005), geophysical structure and hydrological processes (Flipo et al., 2014; Mouhri et al., 2013; Neira et al., 2019; Pasquet et al., 2015) have all been extensively investigated here for the past 50 years. The related hydrological data are available on the ORACLE website (<https://bdoh.irstea.fr/ORACLE/>).

The present study is focused on the Avenelles watershed, a sub-catchment of the Orgeval CZO draining an area of 45 km² (Mouhri et al., 2013). The watershed drains a plateau located 130 m above sea level (Tallec et al., 2015). The climate is temperate and oceanic, with cool and rainy winters (mean temperature 5°C) and dry summers with average temperature close to 20°C. Though the summer months are relatively dry, they are still affected by storms. The annual rainfall is between 600 and 700 mm, and the dominant winds are from the west, especially in winter when fronts move inland from the Atlantic Ocean. Stream flow in the Avenelles River varies substantially by season. At the Avenelles gauging station the average daily water flow is 0.2 m³/s (over the period 1962 to 2016). Low flow rates in the summer are characterized by a discharge of 0.1 m³/s, while flash flood events reach 12 m³/s in the wet season (Tallec et al., 2015). During discharge events, the M elarchez tributary contributes more than 30% of the Avenelles River flow (Figure 1). This value drops to less than 4% in the dry season.

The Avenelles watershed is underlain by sedimentary rocks of Cenozoic age consisting of horizontal layers of limestone, silcrete, clays, and marls forming the most recent strata from the Paris-London sedimentary basin. Two main aquifers supply the stream all year long through several springs (Figure 1). The shallowest formation is a heterogeneous layer a few meters in thickness consisting of loamy silt with high porosity sand lenses called "Limon des Plateaux." Deeper, the Oligocene lacustrine limestone formation hosts a free shallow aquifer (the Brie aquifer) connected to the Limon des Plateaux aquifer. This free aquifer is around 12 m thick, constitutes the main water resource of the basin and supplies several springs. Its water table shows a strong seasonality of up to 3 m (Mouhri et al., 2013) and can reach the surface during the wet seasons. An impermeable green clay layer lies at the bottom of the aquifer. This 5-m thick clay formation separates the Brie aquifer from the deeper and larger Champigny aquifer, which is contained in Eocene limestone and marls with gypsum lenses (Figure 1). Catchment land use is dominated by intensive agriculture (82% of the area) mainly consisting of field crops (wheat, corn, and broad beans), yet irrigation is minimal and there is no widespread groundwater pumping or artificial diversion of stream flow. Nearly 60% of the land surface features enhanced artificial drainage which routes precipitation into the fluvial drainage network. Fertilizer applications are widespread and depend upon the type of crop, with inputs ranging from 120 to 160 kg N ha⁻¹ for wheat and barley to 180 kg N ha⁻¹ for maize, sprayed in February and March (Garnier et al., 2014). Forest and urban infrastructures cover 18% and 1% of the surface area, respectively. The overall combination of agricultural land use practices, a multi-layered aquifer system, and stratified lithology in the Orgeval catchment supports geochemical zonation, which makes this site suitable to evaluate the ways in which solute export couples to dynamic water storage over a variety of hydrological events.

3. Data Acquisition and Treatment

3.1. The Orgeval River Lab

In June 2015, an RL was deployed at the outlet of the Avenelles watershed to measure the contemporaneous concentration of major dissolved species at a high frequency. The RL is an example of the "lab-in-the-field" concept consisting of a climate-controlled structure installed next to the river, performing one complete analysis every 40 min using two Dionex® ICS-2100 ion chromatographs through continuous sampling and filtration of the river water. The RL measures the concentration of all major dissolved species except HCO₃⁻ (Na⁺, K⁺, Mg²⁺, Ca²⁺, Cl⁻, SO₄²⁻, and NO₃⁻). In addition, the RL hosts a series of physico-chemical probes for pH, conductivity, dissolved O₂, DOC, turbidity, and temperature, all recorded every minute. The stream flow of the Avenelles River is recorded at a gauging station adjacent to the RL's location. The design and analytical performance of the RL are detailed in Floury et al. (2017). The utility of such high-frequency RL hydrochemical data sets for solute flux estimates was recently demonstrated by Wang et al. (2024), facilitating novel testing of commonly applied load-estimation algorithms (e.g., Cerro et al., 2014; Diamond & Cohen, 2018; Dornblaser & Striegl, 2009;

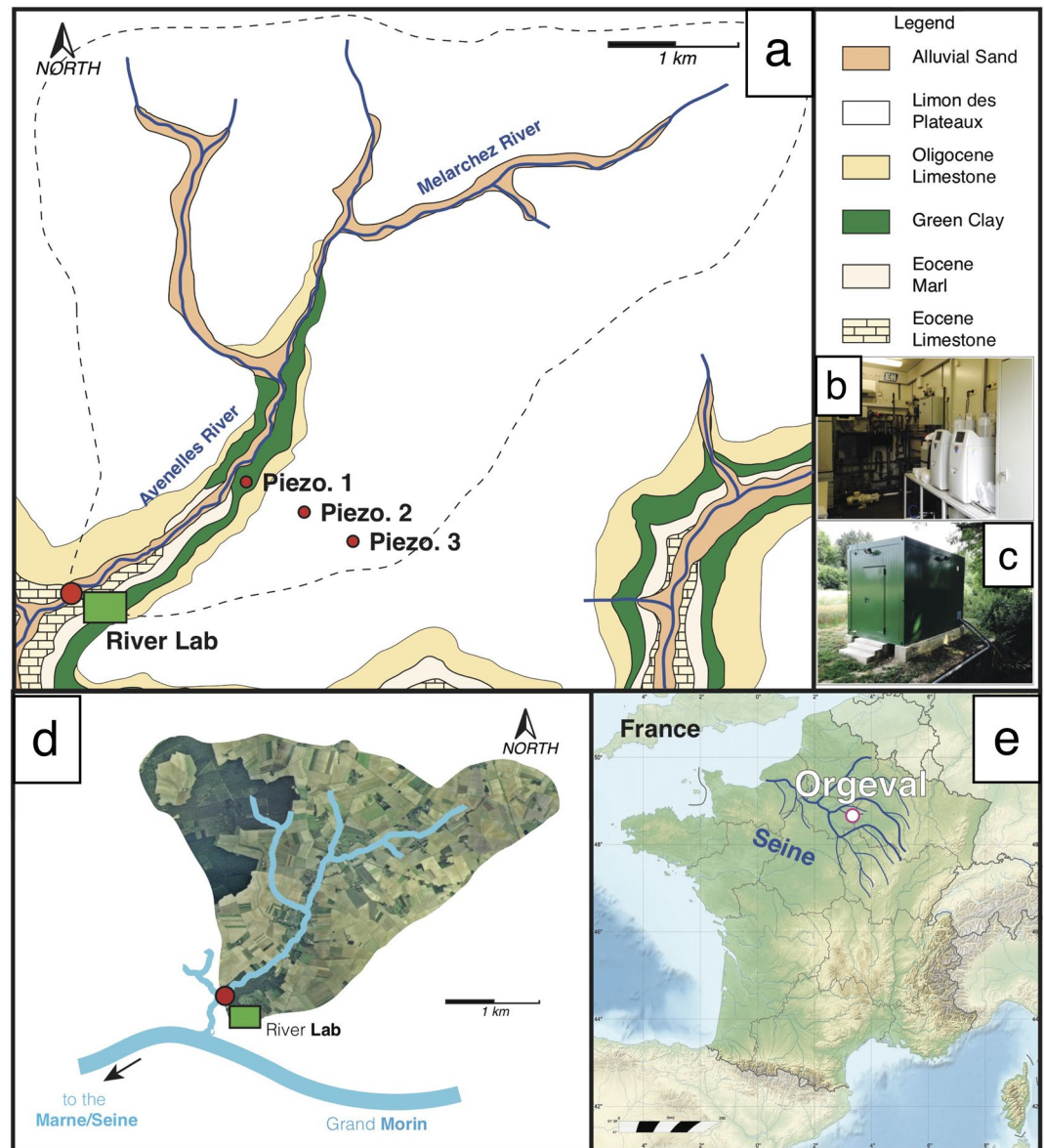


Figure 1. Sampling location. (a) Simplified geologic map of the Avenelles drainage basin. The Avenelles catchment is a sub-watershed in the Orgeval Critical Zone Observatory (CZO). The red dots represent the locations of the River Lab (green rectangle) and of the three piezometers considered in this study. (b) Photo of the inside of the River Lab. (c) Photo of the River Lab from outside. (d) Aerial image of the Avenelles drainage basin showing the land use over the catchment, and position in the hydrologic network of the larger Marne and Seine rivers. (e) Location of the Orgeval CZO in France.

Duan et al., 2012; Park & Engel, 2014; Runkel et al., 2004; Moatar et al., 2017; Minaudo et al., 2019; Musolf et al., 2015).

3.2. Data Set

The present study focuses on five major discharge events recorded over one hydrological year, from the 1 August 2015 to the 1 August 2016 (Figure 2). These five events are chosen because sufficient RL data is available for each of them. From this point forward, we refer to these events as “floods” to distinguish from the shorter period of precipitation that induced these periods of elevated discharge. The end of each flood is defined by a recovery in conductivity to pre-flood values, or when conductivity plateaus over more than half a day (Figure S1 in Supporting Information S1). The five individual flood events are designated by the month during which they took place (November, January, March, April, and June; Figure 2).

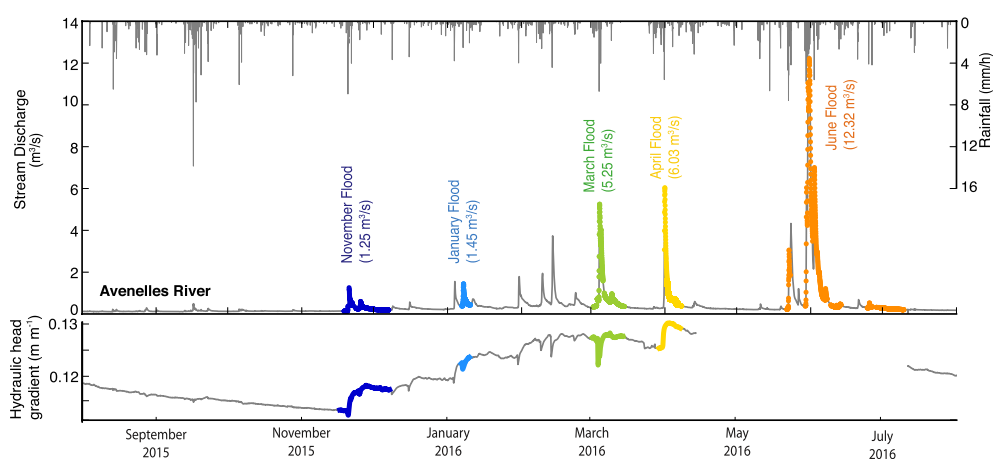


Figure 2. Times series of stream discharge over the hydrologic year 2015/2016 in the Avenelles River, Orgeval Critical Zone Observatory. The rainfall rate is presented on the top of the figure. The hydraulic head gradient between Piezometers 1 and 2 (see Figure 1) is given in the bottom panel. These piezometers are drilled in the free shallow Brie aquifer (see text). The floods (data in color) are the five events selected for the present study. The pressure transducer in piezometer 1 failed after the April flood event and was replaced in early July 2016, causing a gap in the gradient calculation. Each colored dot represents a full analysis (physico-chemical parameters, and seven major solute concentrations) made directly in the field by the River Lab, that is, every 40 min. Each flood event is named for the month during which it occurred. The maximum river discharge recorded over each flood event is given between parentheses.

For each flood, the database (<https://doi.org/10.15454/9PUYPN>) includes major dissolved ion concentrations and all physico-chemical parameters as well as precipitation levels, measured using a rainfall collector located within the catchment. In addition, 3 piezometers drilled in the shallow Brie aquifer record the groundwater level every 30 min. The three piezometers are aligned along a transect perpendicular to the river (Figure 1 and Figure S1 in Supporting Information S1). The first piezometer (Piezometer 1) is located close to the river, drilled in the green clay layers up to a 3-m depth. The two other piezometers (Piezometers 2 and 3) are drilled in the Limon des Plateaux formation at a 6-m depth (Tallec et al., 2015). Finally, an estimation of the PET (potential evapotranspiration) is provided at a daily frequency using the Penman Monteith equation based on several parameters available for the watershed (air temperature, soil moisture, wind and atmospheric pressure; obtained from the database <https://bdoh.irstea.fr/ORACLE/>) (Figure S2 in Supporting Information S1).

3.3. Data Quality

Accuracy, precision, cross-contamination, and instrumental drift of the concentration measurements performed by the RL have been assessed through several tests (Floury et al., 2017). Overall, the precision reached for the concentration measurement itself is better than 0.5% for all species. The one exception is potassium, for which we achieve an estimated 1.2% precision. The instrumental drift between two calibrations (over 2 months) is calculated as the standard deviation of concentration measurements over a series of standard injections. The uncertainty is better than 1% over 1 week and better than 1.7% over 2 months (Floury et al., 2017).

A major concern in continuous field measurement is the possibility of cross contamination between samples. This may occur as a result of the filtration device, particularly when river concentrations are changing rapidly, as typically occurs during flood events (Floury et al., 2017). For the Orgeval River over the hydrological year 2015/2016, the most rapid variations in concentration with time are observed in Cl^- , Na^+ , and SO_4^{2-} . The largest time-derivatives of concentration were recorded during the March and May 2016 flood events, during the rising limb of the hydrograph. The concentration decreased by up to 36% between two measurements (40 min). Tests have been performed to assess cross-contamination effects using injection of a “spike” in concentration (Floury et al., 2017). The corresponding maximum bias we can expect during the five floods considered here is 1.9% and primarily involves 6 measurements for the March flood event (on 4 March 2016 between 10 a.m. and 1.30 p.m.) and 4 measurements for the May flood event (on 30 May 2016 between 1 and 4 a.m.; Figure 3). During the rest of the time across all flood events, the cross-contamination induces a bias estimated to be lower than 0.4%. Therefore, we assume that the cross-contamination is negligible compared to the analytical uncertainty and does not represent an issue for data interpretation. In addition, pure distilled water was regularly injected (at least once a

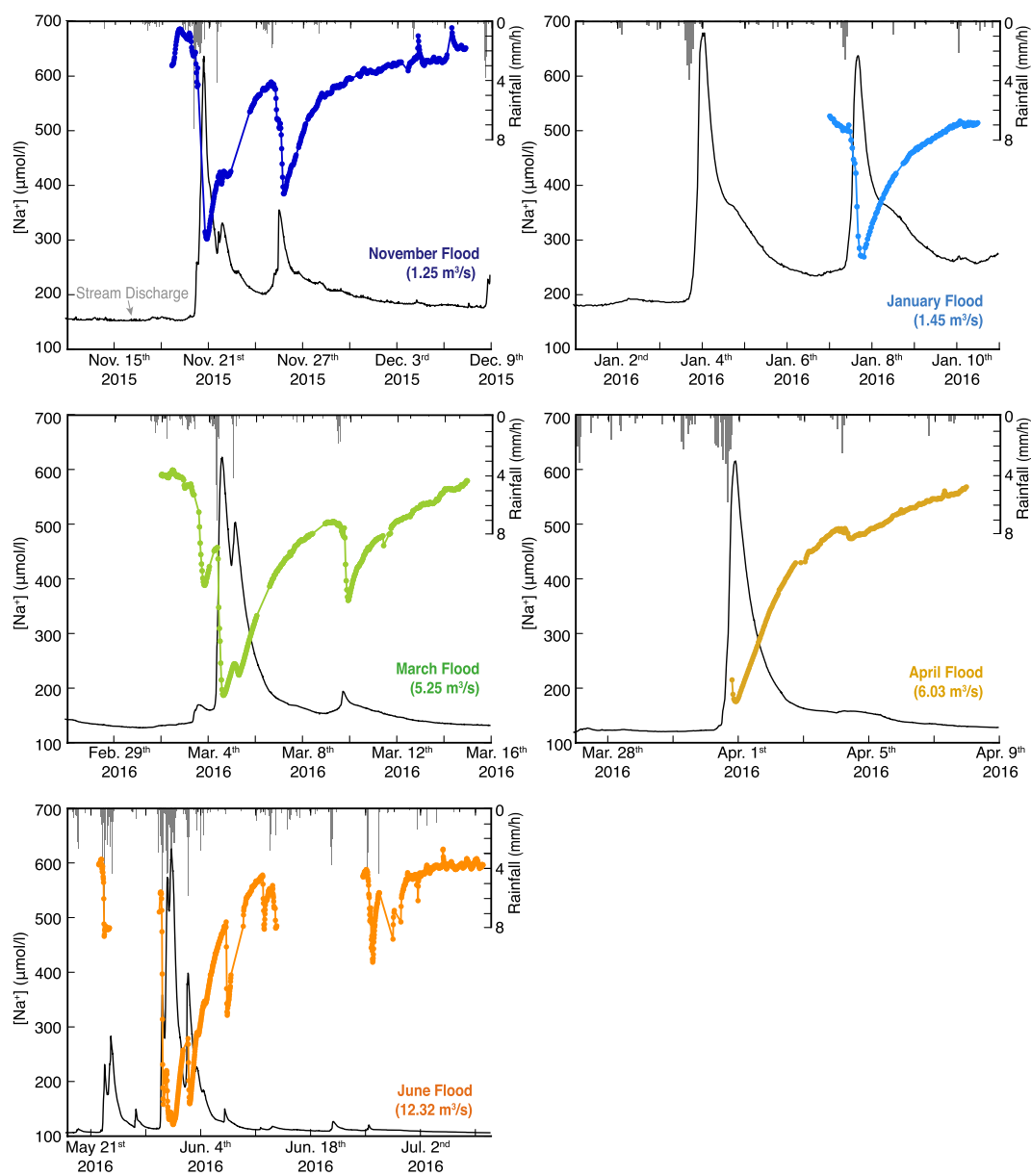


Figure 3. Time series of Na^+ concentrations for each of the five flood events selected over the hydrologic year 2015/2016 in the Avenelles River, Orgeval Critical Zone Observatory. The rainfall rate is presented on the top of the figure. Each colored dot represents a full analysis (physico-chemical parameters, and 7 major solute concentration) made by the River Lab, that is, every 40 min. The black curve in the background represents stream discharge. The maximum discharge values for each event are given between parentheses. Flux-weighted average Na^+ concentration over this time interval is $458 \mu\text{M}$. The measurement uncertainty is smaller than the size of the dots. The number of analyses for the November, January, March, April, and June floods are 563, 238, 804, 250, and 926, respectively. Similar plots for the other species are provided in Figures S3–S8 of the Supporting Information S1.

day) to control the blank level. The blank is checked to ensure values lower than the detection limit for all species. During the January and June flood events this quality control check was not achieved for Ca^{2+} and Mg^{2+} (Floury et al., 2017). Therefore, concentration measurements for Ca^{2+} and Mg^{2+} were discarded for these two flood events.

3.4. Data Analysis

Prior to examination of the relationship between solute availability and export, it is necessary to establish a relationship between water availability and discharge. We employ a simple recession analysis based on the

relationship between Q and its first time-derivative (so-called “ Q - Q dot” analyses; Brutsaert & Nieber, 1977; Kirchner, 2009; Krier et al., 2012; Shaw & Riha, 2012). These models represent the catchment as a nonlinear dynamical system, where stream discharge during recession periods is only dependent on the volume of water stored in a single water pool over the catchment.

The approach begins with the assumption that S is to first order only fed by rainfall (P) and emptied by evapotranspiration (E) and Q .

$$\frac{dS}{dt} = P - E - Q \quad (5)$$

with P , E , and Q all normalized to the catchment surface and given in (m/s), making the dimension of S homogeneous to a length (a depth in (m)), that is, a volume of water normalized by the watershed surface. This necessitates that P is a suitable measure of the water supply to the catchment. It also requires that water loss to deeper aquifers is negligible in the time span considered. For Orgeval these assumptions are reliable given that the main input of water to the stream during storms is the shallow Brie aquifer, which overlies an impermeable green clay layer (Mouhri et al., 2013; Figure 1). In comparison to stream discharge, the fraction of water lost to the deeper Champigny aquifer is negligible at the time scale of a flood event.

Assuming that stream discharge is only dependent on the volume of water stored, a function h can be defined which relates Q and S :

$$Q = h(S) \quad (6)$$

One can then estimate the volume stored as a function of discharge using the reciprocal function (Kirchner, 2009):

$$S = h^{-1}(Q) \quad (7)$$

The evolution of stream flow with storage is given by the derivative of Equation 6:

$$\frac{dQ}{dS} = h'(S) \quad (8)$$

Combining Equations 7 and 8, a function g is defined as:

$$\frac{dQ}{dS} = h'(S) = h'(h^{-1}(Q)) = g(Q) \quad (9)$$

which leads to:

$$g(Q) = \frac{dQ/dt}{dS/dt} = \frac{dQ/dt}{P - E - Q} \quad (10)$$

During periods when $Q \gg E$ and $Q \gg P$, such as nighttime recession periods, Equation 10 can be simplified:

$$g(Q) = -\frac{dQ/dt}{Q} \quad (11)$$

in which case the ratio between the time-derivative of Q and Q itself provides constraints on $g(Q)$, that is, on how discharge varies with water storage in the catchment (Kirchner, 2009).

To constrain $g(Q)$ and thus link storage S and discharge Q at the Orgeval CZO, we exclude all measurements from the ascending parts of the floods and measurements where a non-zero rainfall was recorded ($Q \gg P$). The estimated PET is one order of magnitude lower than stream flow during the three largest flood events (March, April and June) and can therefore be neglected ($Q \gg E$). The recession periods of the November and January flood events occur at night, such that the evapotranspiration is once again negligible.

4. Results

4.1. Hydrology of the Flood Events

The five selected flood events cover the whole hydrological year 2015–2016, from November to June (Table S1 in Supporting Information S1). Together, they represent more than 73% of the total volume of water discharged

by the Avenelles River over the year while they cover less than 30% of the time. The intensity of the five floods ranged over one order of magnitude in terms of peak discharge. The smallest peak value was 1.25 m³/s (November Flood), while the largest was 12.32 m³/s (June Flood) (Figure 2). Between August 2015 and August 2016, cumulative precipitation reached 880 mm, a value 35% higher than the long-term annual average (650 mm) (Tallec et al., 2015). The June flood alone was driven by a rainfall event that constituted ~25% of the total precipitation for the water year (216 mm).

The temporal lag in response of the Avenelles River discharge to an intense rain event is around 8 hr between maximum rainfall and maximum discharge, although this lag changes through the year. The November rain event (rainfall = 74 mm and peak discharge = 1.25 m³/s) mainly recharged the Brie aquifer, as shown by the piezometer levels (Figure 2), whereas similar March and April rain events (respectively 45 mm–5.25 m³/s and 61 mm–6.03 m³/s) occurred when the aquifer was already relatively recharged. In the June rain event, this led to an intense flood (rainfall = 216 mm and peak discharge = 12.32 m³/s; Figure 2).

The first flood event occurred in November 2015 and lasted 10 days (563 analyses). It is the smallest of the five recorded floods (peak discharge 1.25 m³/s) (Figure 2). Due to technical issues, hydrological data are missing for a portion of the first peak's rising limb. The flood event was actually composed of three unique peaks (Figure 3). The conductivity shifted from 750 μS/cm to 450 μS/cm 3 hr after maximum discharge (Figure S1 in Supporting Information S1). It then took more than 10 days for the conductivity to come back to a stable value (680 μS/cm). This flood was the only one which induced a significant long-term decrease in conductivity (~30%).

The second flood event was recorded in January 2016 and lasted 4 days (238 analyses) with a maximum of 1.45 m³/s, following a previous flood having the same intensity 4 days earlier (Figure 3). This January flood discharge consisted of a single peak with a shoulder during the recession period. The conductivity decreased from 670 μS/cm down to 387 μS/cm and was synchronous with the maximum stream flow. The conductivity took more than 3 days to recover to pre-event values.

The third flood event spanned 10 days in March (686 water analyses). The water discharge increased from 0.7 to 5.25 m³/s (650 μS/cm to 321 μS/cm) in less than 8 hr, and 2 hr after the maximum rainfall (Figure 3). This flood was intense and occurred rapidly, as is typical of this watershed when the shallow unconfined Brie aquifer is already recharged.

The fourth April flood event is composed of a single, intense peak stream flow of 6.03 m³/s recorded after 20 days without any prior events (Figure 3). Like the March flood, the timescale over which the April flood initiated was short and the discharge increased rapidly from 0.4 m³/s to 6.0 m³/s within less than 9 hr. The following recession spanned 7 days.

The fifth and largest flood event took place in June (peak discharge 12.32 m³/s) (Figure 2). This event lasted more than one month (926 water analyses). It represents 50% of the total volume of water discharged over the year by the Avenelles River. The last flood with the same intensity recorded in the Avenelles River occurred 25 years ago (Tallec et al., 2015). Only in July did conductivity values return to those found before the flood (from 267 to 680 μS/cm). Ten days of hydrochemical data are missing during the recession period due to technical issues.

4.2. Hydrochemistry of the Flood Events

The range of variation for all major dissolved species concentrations recorded during the five flood events is less than one order of magnitude even during the highest flood in June, whereas the discharge changes by two orders of magnitude (from 0.20 to 12.32 m³/s). This range of variation is also comparable to that observed over longer-term monitoring (Floury et al., 2018) and is consistent with common occurrences of “chemostatic” behavior in streams (Godsey et al., 2009; Li et al., 2017). However, within this broad pattern, almost all chemical elements show characteristic variations that depend on the flood intensity. These may be grouped by similar trends.

Concentrations of Na⁺, Mg²⁺, Ca²⁺, Cl⁻, and SO₄²⁻ present a similar pattern over the five flood events and decrease systematically when discharge increases. The time series of Na⁺ concentrations are presented in Figure 3 as a representative of this group for each of the five floods (similar plots for other species are provided in Figures S3–S8 of Supporting Information S1). No obvious time lag is observed between peak stream flow and minimum concentration except for the November flood. The strongest decrease recorded in Na⁺ concentrations is observed during the June flood, from around 550 to 121 μmol/l, corresponding to a factor of nearly five. For

all other floods, the decrease is within a factor of four. Within this group of species, Mg^{2+} and Ca^{2+} are the most chemostatic (Figures S3 and S4 in Supporting Information S1), and their concentrations decrease by only 40% relative to pre-flood values. The strongest dilution effect on Mg^{2+} and Ca^{2+} concentrations occurred during the April flood event (note that Ca^{2+} data are not available for the January and June floods). SO_4^{2-} concentrations show variations by a factor of six, similar to that of Na^+ (Figure S5 in Supporting Information S1). The maximum range of variation in concentration is observed for Cl^- during the June flood, decreasing by a factor of nine (from 920 $\mu mol/l$ to 102 $\mu mol/l$; Figure S6 in Supporting Information S1).

Variations in the concentrations of K^+ and NO_3^- are more erratic within a given flood and between flood events. Minimum K^+ and NO_3^- concentrations are not systematically associated with discharge maxima (Figures S7 and S8 in Supporting Information S1). Concentrations of NO_3^- show a particularly drastic change in behavior over the five floods. A systematic decrease with discharge is observed during the November and January floods, but concentrations increase by a factor of two during the April flood (Figure S8 in Supporting Information S1). The behavior of K^+ concentration is different from all other species measured as it systematically increases with discharge during all five events. The K^+ concentration outside of flood events is between 65 and 80 $\mu mol/l$. The maximum in K^+ concentration recorded over the five floods occurred during the first part of the November and June floods, reaching 155 and 161 $\mu mol/l$, respectively. During the rest of the June flood event, the K^+ concentration remained largely insensitive to substantial variations in discharge, maintaining values around 100 $\mu mol/l$ (Figure S7 in Supporting Information S1).

The high temporal resolution of our hydrochemical record allows us to detect significant differences in $C-Q$ patterns between the rising and recession periods of each flood, which leads to hysteretic patterns. This is exemplified by the behavior of SO_4^{2-} over the different flood events (Figure 4). Separate $C-Q$ relationships for each flood and solute as illustrated for SO_4^{2-} (Figure 4) are available in Figures S9–S14 of Supporting Information S1. The $C-Q$ relationships of the other six major dissolved species across all five floods indicate that Na^+ , Ca^{2+} , Mg^{2+} , SO_4^{2-} , and Cl^- all follow well-defined trends, particularly for the March, April, and June flood events (Figure 4 and Figures S9–S14 in Supporting Information S1). For Na^+ , Ca^{2+} , Mg^{2+} , and SO_4^{2-} over the five flood events (Figure 5), the ascending limb of the hydrograph is always more chemostatic than the recession and the loops are therefore systematically clockwise. By contrast, the NO_3^- $C-Q$ relationships do not present any systematic pattern over the five floods (Figure S14 in Supporting Information S1). During the March and April flood the NO_3^- $C-Q$ relationship illustrates counter-clockwise loops, with a larger loop in April. The NO_3^- $C-Q$ relationship during the June flood shows several loops. The shapes of K^+ $C-Q$ relationships are similarly complex and vary from flood to flood. During the March and April flood events the K^+ concentration remains almost constant and insensitive to large variation in discharge (Figure S13 in Supporting Information S1).

A standard metric for $C-Q$ relationships is based on a power law, with fit parameters specific to each dissolved species (e.g., Bouchez et al., 2017; Clow & Mast, 2010; Godsey et al., 2009; Ibarra et al., 2016; Knapp et al., 2022; Li et al., 2021; Moquet et al., 2016; Musolff et al., 2015; Rose et al., 2018; Stewart et al., 2022; Wymore et al., 2023):

$$C = \alpha Q^b \quad (12)$$

where C is the concentration of the considered species and Q the discharge of the river. When the b -value is 0, the species is considered perfectly chemostatic (Godsey et al., 2009), and its concentration is essentially independent of Q . A b -value of -1 implies perfect dilution. While this approach does not offer any insight in the mechanisms driving $C-Q$ relationships, we use it as a necessary first step to characterize how the shapes of $C-Q$ relationships vary between solutes among and within floods.

We calculate the b -value for each species over the recession of each flood event (Figure 6; Figures S15–S20 and Table S1 in Supporting Information S1). During the ascending period (not recorded for the November and April floods), the $C-Q$ relationships of Ca^{2+} , Mg^{2+} , SO_4^{2-} , Na^+ , and Cl^- all show erratic patterns and fast changes (Figures 4 and 5; Figures S9–S14 in Supporting Information S1). During these periods, a non-negligible component of precipitation falls directly into the river. In addition, surface runoff, artificial drainage and overland flow are regularly observed at this site and generally expected when discharge exceeds ~ 9 m^3/s (as occurred during the June flood), thus bypassing subsurface water flow paths through the catchment. These features of the system make ascending limbs of storm $C-Q$ relationships strongly sensitive to the exact pace and pattern of event rainfall. For this reason, in what follows we utilize the high temporal resolution of the RL data set to focus our analysis on

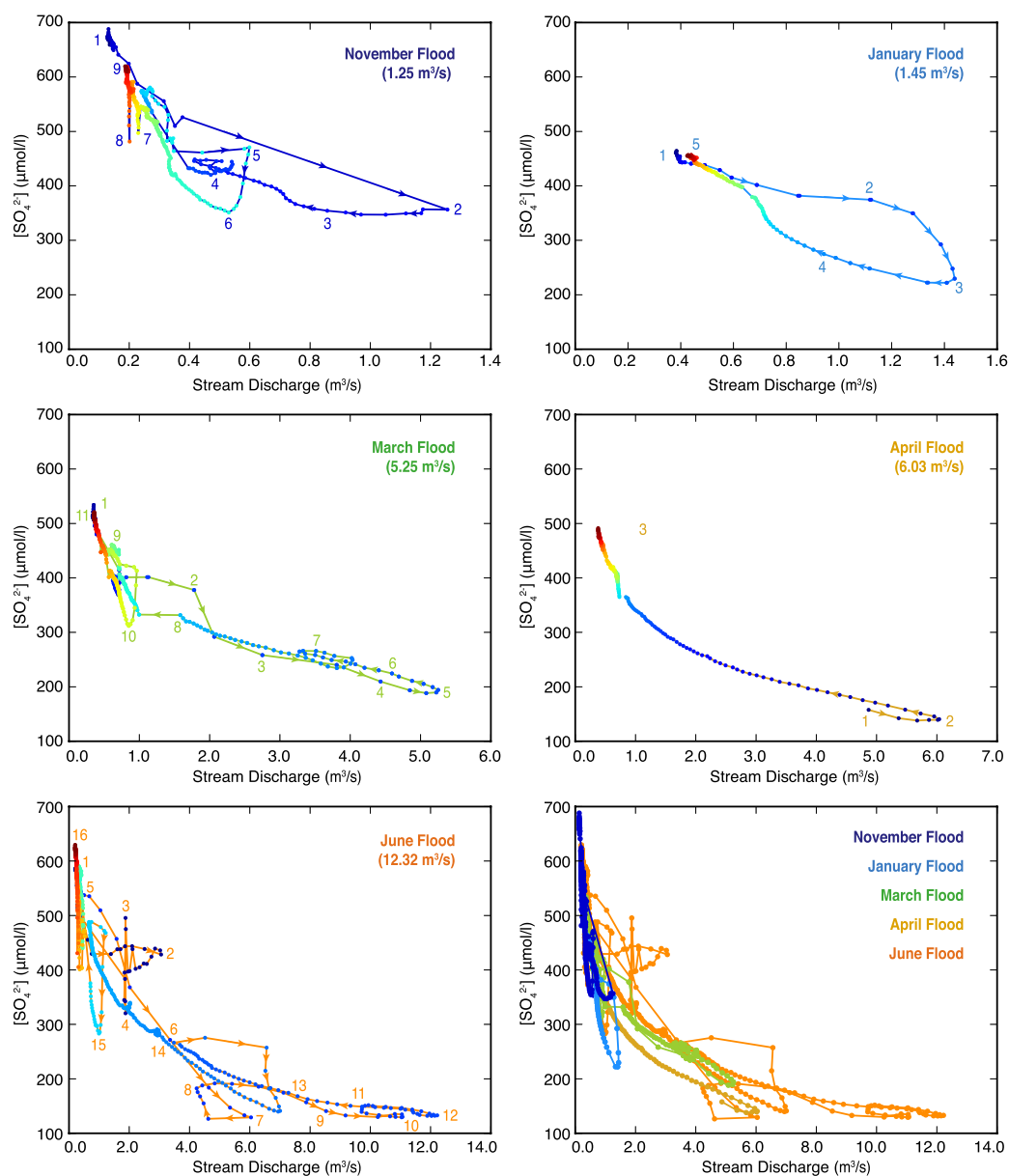


Figure 4. Concentration-discharge (C - Q) relationships for SO_4^{2-} over each of the five flood events selected over the hydrologic year 2015/2016 in the Avenelles River, Orgeval Critical Zone Observatory. Datapoints are colored from blue to red according to the time over the flood event (dark blue = early in the event; dark red = late in the event). Arrows and numbers indicate the progression of time and direction of rotation during the flood. The right-bottom panel summarizes the C - Q relationships for the five floods together. Similar plots are provided for the other species in Figures S9–S14 of the Supporting Information S1.

recession periods. Through this approach we consider the recession period relationships between water and solute export from catchments consistent with previous studies focused on characterization of catchment functioning from hydrological (e.g., Kirchner, 2009) and hydrochemical (e.g., Knapp et al., 2020) perspectives.

In our data set, over a given recession period, the coefficient of correlation for the power law fit is better than 0.90 for most species. The exceptions are NO_3^- and K^+ , for which no simple power-law relationship can reasonably describe the data (Figure 6; Figures S19 and S20 in Supporting Information S1). The b -value closest to chemostasis was recorded for Ca^{2+} during the April flood event at a value of -0.16 (Table 1; Figure 6; Figure S16 and Table S1 in Supporting Information S1). The b -value closest to dilution was recorded for Na^+ during the November flood event at a value of -0.70 (Figure 6; Figure S15 in Supporting Information S1). All b -values for Na^+ ,

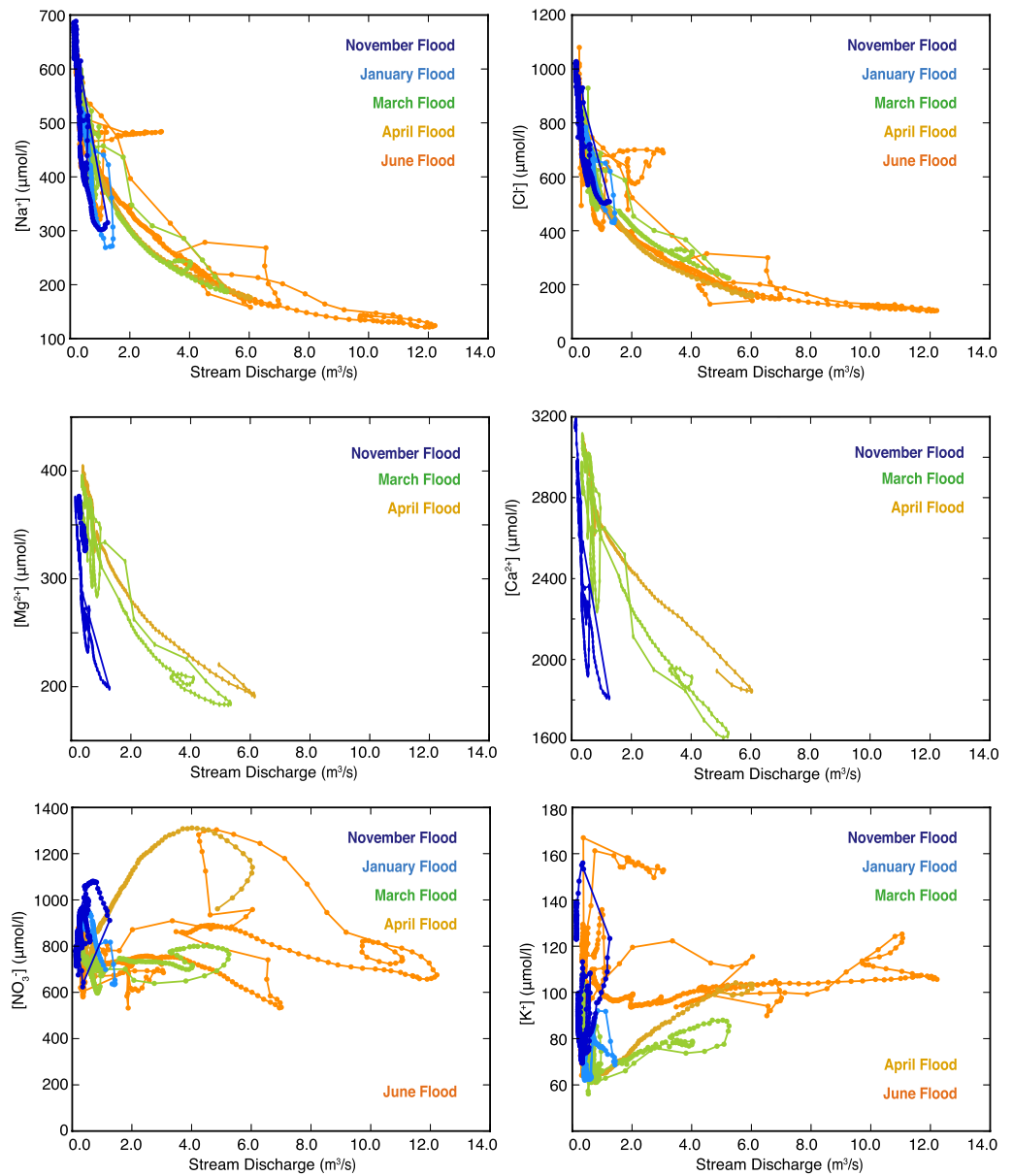


Figure 5. Concentration-discharge relationships for Na^+ , Cl^- , Mg^{2+} , Ca^{2+} , NO_3^- , and K^+ recorded during five floods events over the hydrologic year 2015/2016 in the Avenelles River, Orgeval Critical Zone Observatory. The equivalent plot for SO_4^{2-} can be found in the bottom right panel of Figure 4.

SO_4^{2-} , Ca^{2+} , Cl^- and Mg^{2+} $C-Q$ relationships vary within this range (Figure 6; Figures S15–S18 in Supporting Information S1).

For these five species, the b -value increases (i.e., the $C-Q$ relationship becomes more chemostatic) with flood intensity (Table 1). Na^+ and SO_4^{2-} exhibit the lowest b -values (-0.70 and -0.67 , respectively, during the November flood; and -0.41 and -0.40 , respectively, during the June flood). The most chemostatic species are Ca^{2+} (-0.48 in November to -0.16 in April) and Mg^{2+} (-0.49 in November to -0.31 to -0.25 in April). Amongst all species, Cl^- has the most stable b -value over each of the five recession periods (between -0.58 and -0.44). These observations indicate that at the Orgeval CZO, all stream dissolved species (excluding NO_3^- and K^+) show systematic trends toward “more chemostasis” throughout the hydrological year 2015–2016.

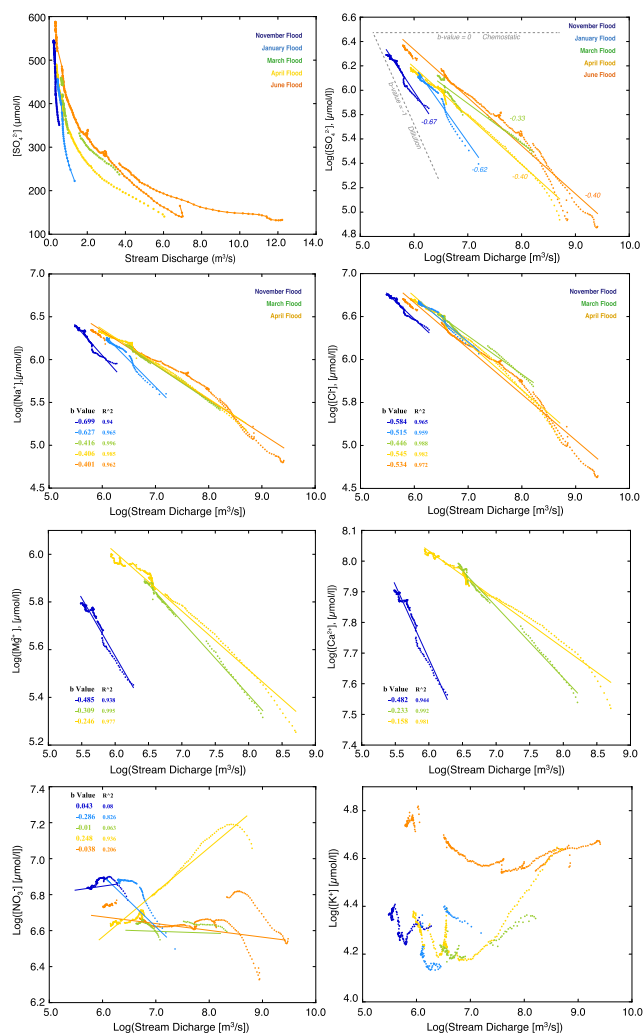


Figure 6. Concentration-discharge (C - Q) relationships for the recession periods of each of the five flood events selected over the hydrologic year 2015/2016 in the Avenelles River, Orgeval Critical Zone Observatory. Here, SO_4^{2-} is used to illustrate these relationships in a linear-linear scale (top left) versus log-log scale (top right). The comparison between scales for the other species is provided in Figures S15–S20 of the Supporting Information S1. The relationships for other solutes are all given in log-log scale and include best-fit trends in this space corresponding to a power-law for the C - Q relationship, Equation 12 for each flood event. The resulting power-law exponent, or “ b -value” is given for each event and each element along with coefficients of determination (see text). The gray dotted lines in the upper right panel represent two extreme scenarios for C - Q relationships: dilution (b -value = -1) and “chemostatic” behavior (b -value = 0).

This latter effect is illustrated by increased water table height in all three piezometers over the water year (Figure S2 in Supporting Information S1) as well as the hydraulic head gradient toward this gaining section of the stream (Figure 2). These data illustrate a systematic increase in the amount of water stored in the catchment as well as the rate of groundwater discharge to the Avenelles. Clearly the age distribution and history of this stored water will influence the time available for solutes to accumulate in the reservoir prior to flood events (Benettin, Bailey, et al., 2017). Several prior studies have suggested larger storage volumes and attendant increases in solubilized mass can “buffer” against variations in concentrations that would otherwise be induced by the supply of new and dilute water during flood events (e.g., Basu et al., 2010, 2011; Godsey et al., 2019; Musolff et al., 2015). Here,

5. Discussion

The high-frequency stream chemistry data collected at the Orgeval CZO over the hydrologic year 2015–2016 using an RL deployment allows us to quantitatively study the relationships between transient water fluxes through the catchment and solute exports by the stream at extraordinary temporal resolution. First-order observations made from this data set confirm previous findings, namely that C - Q relationships of major stream solutes (a) all display hysteresis (e.g., Evans & Davies, 1998; Rose et al., 2018); (b) are element-specific (e.g., Godsey et al., 2009, 2019; Herndon et al., 2015; Knapp et al., 2022; Moatar et al., 2017; Musolff et al., 2015; Pinder & Jones, 1969; Rose et al., 2018; Stewart et al., 2022; Zhi et al., 2019); and (c) are flood-specific (e.g., Knapp et al., 2020; Rose et al., 2018). While statistical multivariate analyses of a large number of event-scale C - Q relationships have proven informative (Knapp et al., 2020; Rice et al., 2004; Rose et al., 2018; Wymore et al., 2019; Zhi & Li, 2020), here we seek to explicitly leverage the high-frequency data sets afforded by the RL over each flood to explore the coupling between water discharge, storage and solute export and the capacity to explain the response of stream solute exports as a result of these shifts. This is made possible by the diversity of “flood regimes” covered by our data set at the Orgeval CZO, ranging from a relatively moderate flood triggered by a rain event affecting a depleted shallow aquifer at the beginning of the rainy season (November 2015), to a major flood triggered by a large storm event on a well-recharged aquifer at the end of the rainy season (June 2016). Recognizing that our record covers only the hydrological year 2015–2016, we offer this high-frequency tracking of a sample set of flood events over a large range of duration and intensity as a means of surveying the behavior of a complex system characterized by geochemical zonation.

In the following discussion, we first show how recession C - Q relationships shift over the year depending on flood regime and antecedent conditions, and then extend these relationships to test the link between water and solute export by streams during flood events as driven by changes in water storage within the system.

5.1. Variation in Flood Recession C - Q Relationships at the Orgeval CZO: Dependence on Antecedent Conditions and Practical Consequences

Examination of the general trends displayed by C - Q relationships through for example, power-law fits lack a mechanistic foundation, but nevertheless lend valuable insight into how closely water dynamics and solute mobilization are linked. Values of the b -exponent of recession C - Q relationships (Equation 12) indicate that at the Orgeval CZO, most stream dissolved species (excluding NO_3^- and K^+) become “more chemostatic” throughout the hydrologic year 2015–2016, that is, as flood events become larger and as the aquifer fills.

Table 1
Characteristics of the Five Flood Events Selected Over the Hydrologic Year 2015/2016 in the Avenelles River, Orgeval Critical Zone Observatory

	Flood event									
	November		January		March		April		June	
	Max. discharge (Q_{peak} , $\text{m}^3 \text{s}^{-1}$)									
	1.25		1.45		5.25		6.03		12.32	
	Power law exponent of C - Q relationship (b -value) (R^2)									
SO_4^{2-}	-0.67	(0.98)	-0.75	(0.85)	-0.28	(0.46)	-0.40	(0.99)	-0.39	(0.99)
Ca^{2+}	-0.48	(0.94)			-0.23	(0.99)	-0.16	(0.98)		
Mg^{2+}	-0.48	(0.94)			-0.31	(0.99)	-0.25	(0.98)		
Na^+	-0.70	(0.94)	-0.63	(0.97)	-0.42	(0.99)	-0.41	(0.99)	-0.40	(0.96)
Cl^-	-0.58	(0.97)	-0.52	(0.96)	-0.45	(0.99)	-0.54	(0.98)	-0.53	(0.97)
NO_3^-	0.04	(0.08)	-0.28	(0.82)	0.01	(0.06)	0.25	(0.94)	-0.04	(0.21)
K^+	-0.14	(0.51)	0.20	(0.56)	0.09	(0.88)	0.08	(0.53)	-0.04	(0.64)
	Slope of dQ/dt - Q relationship (a_Q , 10^{-5} s^{-1}) (R^2)									
	6.99	(0.90)	4.77	(0.93)	1.90	(0.97)	2.03	(0.96)	1.33	(0.96)
	Q -intercept of dQ/dt - Q relationship (Q_0 , $10^{-8} \text{ m}^3 \text{ s}^{-1}$)									
	1.40		1.47		1.56		1.45		1.35	
	Ratio between Q_{peak} and Q_0 (β_Q , dimensionless)									
	2.0		2.2		7.5		9.2		20.3	

Note. An expanded version of this Table is available in Table S1 of Supporting Information S1.

we make no a priori assumption about the relationship between water storage volumes and solute load within the near-surface environment. We return to this point in subsequent sections of the discussion.

With our high-frequency data, these power law fits also offer a means to examine tendencies toward chemostasis versus dilution within a single flood event recession, using a sliding window (group of 15 successive analytical points in time, which was chosen as an optimization between sufficient resolution to view variations in b -values and sufficient data density to support a robust power-law fit). For all species, b -values are not constant during a single flood event and generally fall closer to a dilution trend (lower b -value) at the maximum of discharge followed by more chemostatic behavior later in the recession (Table 1; Figure 6; Table S1 in Supporting Information S1). For example, during the June flood, the b -value for Na^+ changes more over a single recession period (-0.78 to -0.31 for an overall value of -0.41) than over the five flood events. During the April flood, the b -value of Mg^{2+} evolves from -0.40 to -0.16 at the end of the recession. A similar change is also found for SO_4^{2-} (from -0.76 to -0.30) and Cl^- (from -0.92 to -0.40). Such changes in the b -value might reflect how water flow paths evolve during the recession period itself. For example, at peak discharge, dilution is maximal (lowest b -values), which could suggest a less efficient buffering of dilution effects (as discussed above) by the water already stored in the catchment. Similar effects of variable fluid travel time between the stream and solute sources within the catchments have been discussed for DOC and a number of rock-derived solutes by Herndon et al. (2015), and for DOC and nitrate by Vaughan et al. (2017).

A practical implication is demonstrated by these high-frequency concentration data. When multiple events are aggregated into an overall C - Q relationship combining many individual storms, parameters extracted from empirical (e.g., power law) fits are strongly skewed by the largest flood events driving C values at very high Q , and therefore correspond to very specific hydrological conditions—that is, when the aquifer is already relatively full. As a result, parameter values obtained from a single fit to a collection of multiple storms is unlikely to represent the variety of water flow paths and solute sources in a given catchment that would most appropriately describe baseflow C - Q behavior or even the C - Q patterns of individual precipitation events (e.g., Fazekas et al., 2020). The high-frequency monitoring afforded by the RL deployment offers an important opportunity to better characterize - and thus potentially understand - the response of stream solute export to shifts in hydrological regime through a detailed sampling of individual flood events occurring under a broad variety of hydrologic conditions.

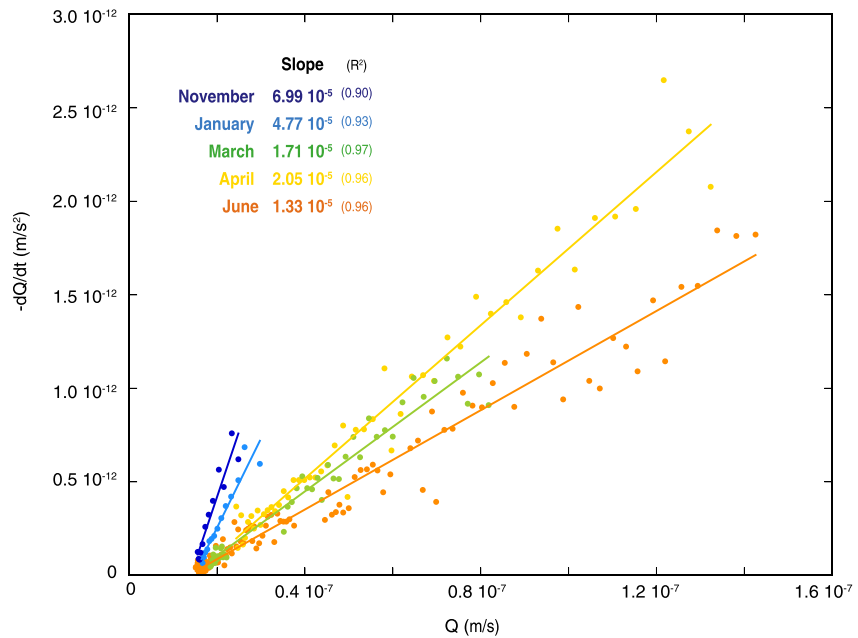


Figure 7. Negative of the first time-derivative of river discharge ($-dQ/dt$) versus river discharge (Q) (here normalized to catchment area) for each of the recession periods of the five flood events selected over the hydrologic year 2015/2016 in the Avenelles River, Orgeval Critical Zone Observatory. Lines correspond to linear best-fits for each of the five flood events (slope and coefficient of determination R^2 are given in the top-left corner of the figure).

5.2. Linking Water and Solute Export During Flood Events

Previous studies have shown that flow paths contributing to a stream can vary over seasonal time scales, as well as during a single flood event (Calmels et al., 2011; House & Warwick, 1998; Koenig et al., 2017; Stallard & Murphy, 2014). We now evaluate whether the present C - Q relationships are essentially describable as a reflection of the relationship between water discharge and water storage in the catchment, or if the data suggest activation of distinct chemical reservoirs during a given flood event. Such changes in storage can be triggered by the activation/deactivation of flow paths; while such pre-existing solute pools might be present in “water pockets,” or as readily mobilizable, (e.g., exchangeable) species (e.g., Seibert et al., 2009; Thompson et al., 2011). In this framework, chemical reactions (such as mineral dissolution/precipitation) do not directly drive event-scale recession C - Q relationships. In what follows, we explore the extent to which mobilization of multiple solute pools is necessary to describe event C - Q behavior for the Orgeval system using a simplified recession analysis (Section 3.4).

5.2.1. The Relationship Between River Discharge and Water Storage at the Orgeval CZO

For each flood event, a linear regression (Figure 7) between Q and dQ/dt with a non-zero Q -intercept accurately matches the data ($R^2 > 0.9$ for all individual flood events).

$$-\frac{dQ}{dt} = a_Q(Q - Q_0) \quad (13)$$

Here $a_Q > 0$ (in unit s^{-1}) is the flood-specific slope of the relationship in Figure 7, and Q_0 (in m/s) is the Q -intercept of the $-dQ/dt$ - Q linear trend. We note that an equivalent of Figure 7 in log-log space did not display linear trends (Figure S21 in Supporting Information S1). In our approach, we consider each flood event individually, meaning that the fit parameters a_Q and Q_0 differ from one flood to the next, which is different from the original approach of Kirchner (2009). In doing so, we allow for variations in recession curve characteristics due to differences in precipitation and infiltration rates of each storm as well as seasonal differences stemming from factors such as evapotranspiration, aquifer storage and soil moisture (e.g., Shaw & Riha, 2012). However, as discussed below, the five best-fit lines converge to approximately the same intercept point ($Q = Q_0$) indicating a relatively consistent base flow rate of approximately 1.35 – 1.55×10^{-8} m/s (or around 0.6 – 0.7 m³/s) outside of the flood events (Table S1 in Supporting Information S1). In reality, Q_0 varies

over the course of the year from November to June as the system transitions across wet and dry seasons, but this rate of change is small and thus negligible in the context of our flood recession analysis. For the present purpose, application of Equation 13 to the five individual storms indicates that Q_0 may be reasonably treated as flood-invariant.

The linear behavior of Equation 13 is compatible with an exponential decrease of Q with time (Figure 3). However, it should be emphasized that in the case of the Orgeval CZO, at the end of the recession, Q does not tend to a 0-value. This is distinct from the case of a “linear response” where Q would simply scale as S (Kirchner, 2009). The fact that the intercept of the lines described by the flood data in Figure 7 are not equal to 0 reflects the perennial nature of the Avenelles River: after a given flood, discharge never reaches 0. This implies that baseflow is supplemented by water in addition to that involved in event-scale discharge response. This inference is consistent with the geological background of the Orgeval CZO, where aquifers hosted in sedimentary rock reliably supply most of the water to the river throughout the year (Figure 2; Floury et al., 2018).

Across our five floods, the slope of the linear best fit (a_Q , Equation 13) varies from $7.0 \times 10^{-5} \text{ s}^{-1}$ for the November flood event to $1.3 \times 10^{-5} \text{ s}^{-1}$ for the June flood event (Figure 7; Table S1 in Supporting Information S1). The slopes are significantly distinct between flood events (as observed by Shaw and Riha (2012)), and decrease with the intensity of the flood. We observe no systematic deviation between the data and our linear best-fits across the Q range, reinforcing the validity of a linear best-fit for the $dQ/dt-Q$ relationships at this site. In addition, it is important to note that a single linear $dQ/dt-Q$ relationship for the five floods combined could provide a satisfactory first order fit to the whole data set, but the fit parameters would be heavily influenced by the largest flood events and would obscure the specific response of each flood.

Although catchment $dQ/dt-Q$ relationships have been examined in many past studies, we are unaware of any prior literature reporting a linear relationship between Q and its first time-derivative with a non-zero intercept. For example, the study by Ceola et al. (2010) considered a variety of linear least squares regression methods applied to 13 different catchments, but only in $\ln-dQ/dt \ln-Q$ space (as noted above, our data do not produce satisfactory linear trends in such space; Figure S21 in Supporting Information S1). One possibility to translate such a $dQ/dt-Q$ relationship into a $q = h(S)$ relationship (short of calibrating a full SAS-type model with the need for extensive long-term tracer data) would be to consider that stream discharge at Orgeval consists of the sum of two separate water fluxes (a) a deep water source contributing a discharge Q_0 that remains constant over the flood event, and (b) a shallower water pool displaying a purely linear response in discharge to storage (e.g., Fovet et al., 2015; Wittenberg, 1999). Such an approach was suggested using coarser sampling frequency by Stewart et al. (2022) and validated based on geochemical characterization of shallow (soil water) and deep (groundwater) samples. We note that such a “shallow and deep” hypothesis is distinct from the earlier two-water worlds hypothesis advanced by McDonnell (2014) and we make no assertion of water or solute partitioning due to ecophysiological separation at the Orgeval catchment. Here, we lack the constraints necessary to assign geochemical characteristics to the storage volumes that would supply these fluxes, but we are leveraging a much higher frequency $C-Q$ data set specifically over the recession period of these events. Hence, to extend our recession analysis to $C-Q$ behavior, we provide a new mathematical solution for Equation 13 that considers a single, “continuous” water storage for the whole catchment based on the linear relationship constrained by our event-scale discharge data. By combining Equations 9 and 13 we reach a specific expression for dS :

$$dS = \frac{1}{a_Q} * \frac{QdQ}{Q - Q_0} = \frac{d(Q - Q_0)}{a_Q} + \frac{Q_0}{a_Q} * \frac{d(Q - Q_0)}{Q - Q_0} \quad (14)$$

which can be integrated between S and S_{peak} (maximum water storage in the catchment, corresponding to the beginning of the recession, i.e., to peak discharge):

$$S - S_{\text{peak}} = \frac{(Q - Q_{\text{peak}})}{a_Q} + \frac{Q_0}{a_Q} \ln \left(\frac{Q}{Q_{\text{peak}}} \right) \quad (15)$$

where Q_{peak} is peak discharge, that is, when $S = S_{\text{peak}}$. This equation can be made non-dimensional for ease of manipulation:

$$s = q - 1 + \frac{1}{\beta_Q} \log(q) \quad (16)$$

using the following dimensionless variables (s , q) and parameter (β_Q):

$$\begin{aligned} s &= a_Q \frac{S - S_{\text{peak}}}{Q_{\text{peak}}} \\ q &= \frac{Q}{Q_{\text{peak}}} \\ \beta_Q &= \frac{Q_{\text{peak}}}{Q_0} \end{aligned} \quad (17)$$

Here Equation 15 offers a dimensional estimate of water lost from storage over the recession limb of the flood hydrograph ($S - S_{\text{peak}}$, units of meters). When recast into Equation 16, s offers an estimate of dimensionless storage, that is, a relative instantaneous storage normalized to Q_{peak}/a_Q , which varies from 0 at the beginning of the recession period to $a_Q \frac{S_{\text{min}} - S_{\text{peak}}}{Q_{\text{peak}}}$ (a negative value) when the stream has returned to base flow Q_0 . q is a dimensionless discharge (normalized to the peak discharge Q_{peak}), varying from 1 at the beginning of the recession period to $1/\beta_Q$ at the end of the recession. β_Q (≥ 1) is a fixed parameter for a given flood and serves as an indicator of the “intensity” of the flood (i.e., a ratio of peak discharge Q_{peak} to baseflow Q_0).

Equation 16 and the associated translation to q as a function of s (see Supporting Information S1 for detailed derivation) allow us to produce q - s relationships (Figure S22 in Supporting Information S1) for our five floods which can be interpreted broadly within this model framework. First, for a given flood, the discharge response (i.e., the slope in Figure S22 of Supporting Information S1) is greatest for high storage values (in other words, high discharge values, such as those observed at the beginning of the recession), most likely reflecting fast export of water when the aquifer and shallow water pools have been replenished by new water from precipitation (Figure 2). Second, the q - s curves of the three late floods (March, April, and June) in Figure S22 of Supporting Information S1 lie below those of the two early floods (November and January). This observation does not inherently imply that water storage in the catchment was smaller for the early floods, because each result in Figure S22 of Supporting Information S1 is normalized to event-specific non-dimensional values (Equation 17), such that only the slope of the trends offers a meaningful comparison between floods. The difference between the two groups of floods can be qualitatively linked to the antecedent water storage conditions within the catchment. The November and January floods lead to significant recharge of the shallow Brie aquifer, as suggested by the large increase in piezometer water levels during these early events (Figure S1 in Supporting Information S1). In contrast, the three floods that occurred later in the year were associated with much more water in the shallow aquifer and produced a comparatively larger discharge response (Figure 2).

To summarize, our recession analysis of discharge data at the Orgeval CZO suggests that the water storage-discharge relationship varies across the year, depending on the duration and intensity of storms as well as the antecedent conditions of the system. This association is demonstrated by tracking the level of the shallow Brie aquifer before each of the flood events begins (Figure 2 and Figure S1 in Supporting Information S1). In the following, we use this simplified model as a point of comparison to consider where the assumption of a single storage volume breaks down in extension to C - Q relationships over flood event recessions.

5.2.2. C - s Relationships Over Recession Periods

Both dimensional (Equation 15) and non-dimensional changes in storage (Equation 16) for each of the events are obtained from the corresponding Q records using parameters appropriate to each flood. The translation to storage loss over the course of the storm offers an estimated length of water evacuated from the system, while rescaling to a dimensionless value essentially normalizes the values of Q_{peak} recorded for each storm to a common starting point (Figure 8). The evolution of s to more negative values is then determined by the starting point Q_{peak} for each flood, given that Q_0 is flood-invariant.

Then, in combination with the high-resolution data record of C - Q behavior over a variety of flood events using the RL deployment, and the benefit of well-constrained recession curves, we may consider when and for which solutes we incur the greatest error in assuming that C - Q relationships are driven only by changes in s , such that C_s can be considered homogeneous (Equation 4).

Beginning with dimensional change in storage, we encounter the interesting result that relatively comparable levels of water were evacuated (0.2–0.3 m) despite the large range of precipitation, duration, and hydrograph

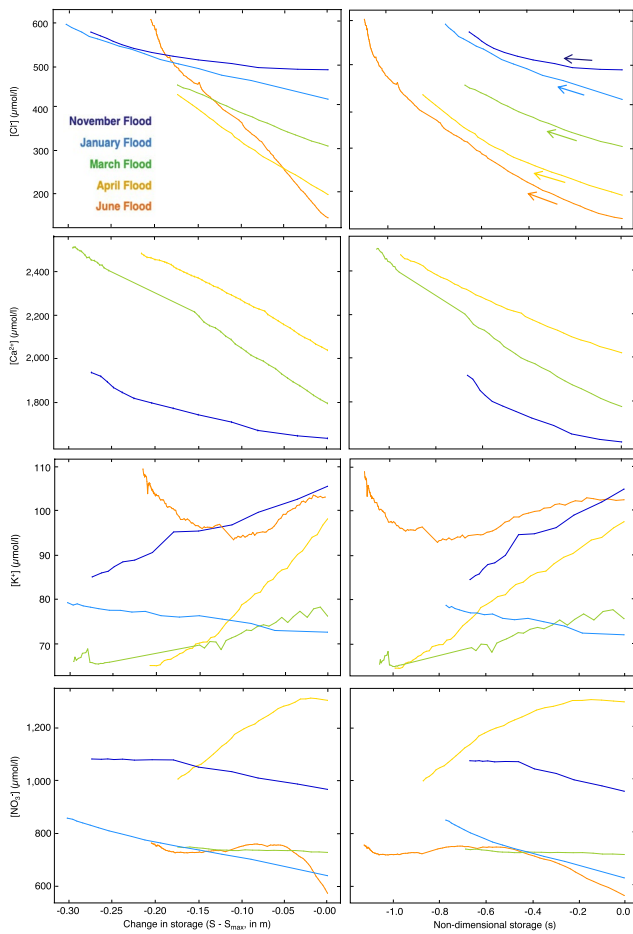


Figure 8. Concentration-storage (C - s) relationships for each of the recession periods of the five flood events selected over the hydrologic year 2015/2016 in the Avenelles River, Orgeval Critical Zone Observatory, from top to bottom Cl^- , Ca^{2+} , K^+ and NO_3^- . Left column: change in dimensional storage ($S - S_{\text{max}}$ in meters); right column: non-dimensional storage (s). January and June events are omitted for Ca^{2+} because the corresponding data did not satisfy quality criteria (see text). Corresponding plots for Na^+ , Mg^{2+} and SO_4^{2-} are provided in Figure S23 of Supporting Information S1.

response across the recession periods of these 5 flood events (Figure 8). In fact, this is consistent with the behavior of the piezometer water levels (Figure S1 in Supporting Information S1), in which the earliest November event produced a rise in the water table of approximately the same magnitude (~ 1 m) as the much larger April and June events. In the period where available piezometer data allowed us to calculate the hydraulic head gradient to the stream it is evident that the earlier, smaller events are impacting a lower storage volume at the beginning of the wet season, while the later, larger events are adding to a much larger storage, such that the shifts in gradient remain relatively consistent ($\sim 5 \text{ mm m}^{-1}$) across these disparate flood events. Moving to the dimensionless C - s space, s during each storm is now normalized to an individual value of a_Q/Q_{peak} . In this space each range of s is specific to a given flood, implying that the same change in dimensionless storage can (and does; Figure S1 in Supporting Information S1) correspond to different levels of absolute storage across the water year. Though this introduces more complexity in the interpretation of the parameter value, it allows us to compare the sensitivity of individual solute concentrations to changes in storage across these 5 flood events despite wide variations in (a) the volume of subsurface water stored and (b) peak discharge.

In this space, solute concentrations of most of the major ions (Cl^- and Ca^{2+} shown in Figure 8; Na^+ , SO_4^{2-} and Mg^{2+} shown in Figure S23 of Supporting Information S1) at peak discharge (Q_{peak} and $s = 0$) are inversely correlated with the size of the flood. We note that Cl^- displays a behavior generally similar to that of Na^+ and other major ions despite the fact that this anion is often considered non-reactive at such low concentrations (Figure 8; Figure S23 in Supporting Information S1). For example, in November, peak discharge Cl^- concentrations are $>500 \mu\text{mol/L}$, while at the start of the June recession this value is $<200 \mu\text{mol/L}$; for Na^+ these values are >300 and $<200 \mu\text{mol/L}$, respectively. Such stark contrast reflects both the seasonal evolution from dry to wet conditions and the size of the discharge events. Furthermore, this distinction reflects an important starting point for the recovery of these solutes through the recession period of each flood, which is closely tied to the diluting effects of the floods on concentrations. For example, even for relatively small events, the b -value for Na^+ is roughly -0.7 (Figure 6), while for the largest flood in June it reaches -0.4 . This implies that at the beginning of the recession period (at Q_{peak} and $s = 0$), solute concentrations are very low in the stream compared to what must be evacuating from the subsurface.

As direct inputs of rainwater and overland flow are replaced by subsurface drainage, these concentrations rapidly increase as the solutes are efficiently evacuated from a (sub)component of the storage volume that can produce a relatively high solute flux. Cl^- concentrations show less convergence to a common value at Q_0 than those of Na^+ . This may imply seasonal differences in baseflow Cl^- concentration, or incomplete recovery to baseflow values over the recession interval defined based on a return to stable conductivity values. In pristine environments, relatively high variability in Cl^- is anticipated given that this solute is not strongly regulated by geochemical reactivity. However, in this agricultural setting, anthropogenic effects such as fertilizer inputs or domestic waste disposal may become significant. In either case, our data illustrate that Cl^- solute sources do not precisely mimic those of Na^+ .

Continuing with the unique normalization offered by recasting C - Q into C - s space using the linear dQ/dt - Q relationship documented in this system, the C - s behavior of Ca^{2+} (Figure 8) and Mg^{2+} (Figure S23 in Supporting Information S1) are similar to one another, and distinct from those of Na^+ and Cl^- . Unfortunately, the data quality standards were not satisfied for these cations during the largest April and June floods (Section 3.3; Floury et al., 2017) and must be omitted from subsequent analysis. For the remaining data, the concentrations at maximum discharge no longer organize chronologically over the water year. Rather, they all appear to cluster in a similar range of values, with the November storm falling slightly below March and April. The b -values of the

larger floods are more chemostatic than Na^+ and Cl^- , yielding values of -0.23 in March and -0.16 in April for Ca^{2+} (Figure 6). The corresponding C - s behavior of these solutes are not as dramatic in their recovery. This contrast suggests a combination of factors: (a) lesser extent of dilution implies easier recovery to baseflow solute concentrations; and (b) the process of recovery is more consistent with the evacuation of a single, uniform fluid storage reservoir, as may be expected for uniformly distributed solute compositions such as Ca^{2+} and Mg^{2+} in Orgeval, where an Oligocene lacustrine limestone formation hosts the shallow Brie aquifer.

SO_4^{2-} behavior (Figure S23 in Supporting Information S1) is generally consistent with that of Na^+ and Cl^- , but the chronological ordering of concentration differs. For example, during the March flood, SO_4^{2-} was less diluted than Na^+ and Cl^- (b -value of -0.33 ; Figure 6) and the corresponding C - s relationship does not exhibit as steep of a gradient, suggesting behavior closer to that of Ca^{2+} and Mg^{2+} during the conditions of this one event. Multiple years of monitoring will be necessary to document the reproducibility of this behavior, but it opens the possibility for event-specific, or season-specific periods in which stored solute pools are more or less uniform for a given element.

The C - Q behavior of species that are commonly applied as fertilizers, such as NO_3^- and K^+ , are highly erratic (Figure 5) to the point that meaningful application of power-law relationships based on Equation 12 are largely impeded. Such erratic C - Q behavior translates into what appears to be relatively clearer corresponding C - s relationships. The key here is that the dQ/dt - Q behavior of these floods (Figure 7) is essentially being reproduced with the inclusion of additional scatter due to a lack of discernible pattern in the flood NO_3^- and K^+ concentrations. When this behavior is translated into the C - s space, the result is distinct from all other solutes presented in Figure 8 and Figure S23 of Supporting Information S1. There is no systematic relationship between size of flood, wet or dry antecedent conditions and concentration at maximum discharge. For K^+ , the November, April and June floods all show similarly high starting concentrations, which may be associated with agricultural land management practices. In contrast, only the November and April floods start at high values for NO_3^- . Such behavior is consistent with solutes that are readily mobilized from the land surface during overland flow and rapid routing of surface water to the stream through the artificial drainage networks (Li et al., 2021).

In total, the reconstructed C - s relationships based on recession analysis allow us to account for a diversity of recession C - Q relationships, as observed in various data sets (e.g., Godsey et al., 2009, 2019; Herndon et al., 2015; Knapp et al., 2020; Moatar et al., 2017). In addition, recession C - Q and C - s relationships show significant and systematic differences between solutes that appears to be related to one or several controlling factors:

- The relationship between concentrations at peak discharge and season, or antecedent hydrological conditions. For some solutes (e.g., Na^+ , Cl^- , SO_4^{2-}) the first floods following the dry season appear to carry significantly higher concentrations than those occurring later in the water year.
- The overall size of the discharge event which appears to regulate the degree to which these same solutes are diluted and hence the extent to which they must recover over the recession period.
- The extent to which these solutes are readily solubilized, for example, the high concentrations of Ca^{2+} and Mg^{2+} associated with a limestone lithology.
- The extent to which these solutes are derived from anthropogenic surface applications associated with fertilizers and other soil amendments, which further impose heterogeneity in the vertical distribution of these solutes, and may even invoke lateral variations in both sources and connectivity (Arora et al., 2020; Herndon et al., 2015)

Each of these factors influences the relationship between water storage, subcompartments of the water storage and the mass of solutes stored therein. In principle, solute-specific C - s relationships could be constrained through adjustment to individual behavior. However, in the absence of independent constraints on the relationship between water and solute storage that could validate this approach, the utility of such adjustment is not obvious. Future work could help to better constrain these relationships, for example, using piezometer levels (to estimate water storage) and groundwater sampling (to estimate solute storage) distributed over the catchment (Stewart et al., 2022).

5.2.3. An Interpretation for the Inferred Relationships Between Elemental Storage and Solute Export

Above, we explored the ability of a simplified relationship between water released from storage (s) and a homogeneous solute composition to explain the diversity of shapes observed in recession C - Q relationships for various solutes at the Orgeval catchment. We observe that the inter-flood shape of C - s relationships can vary widely

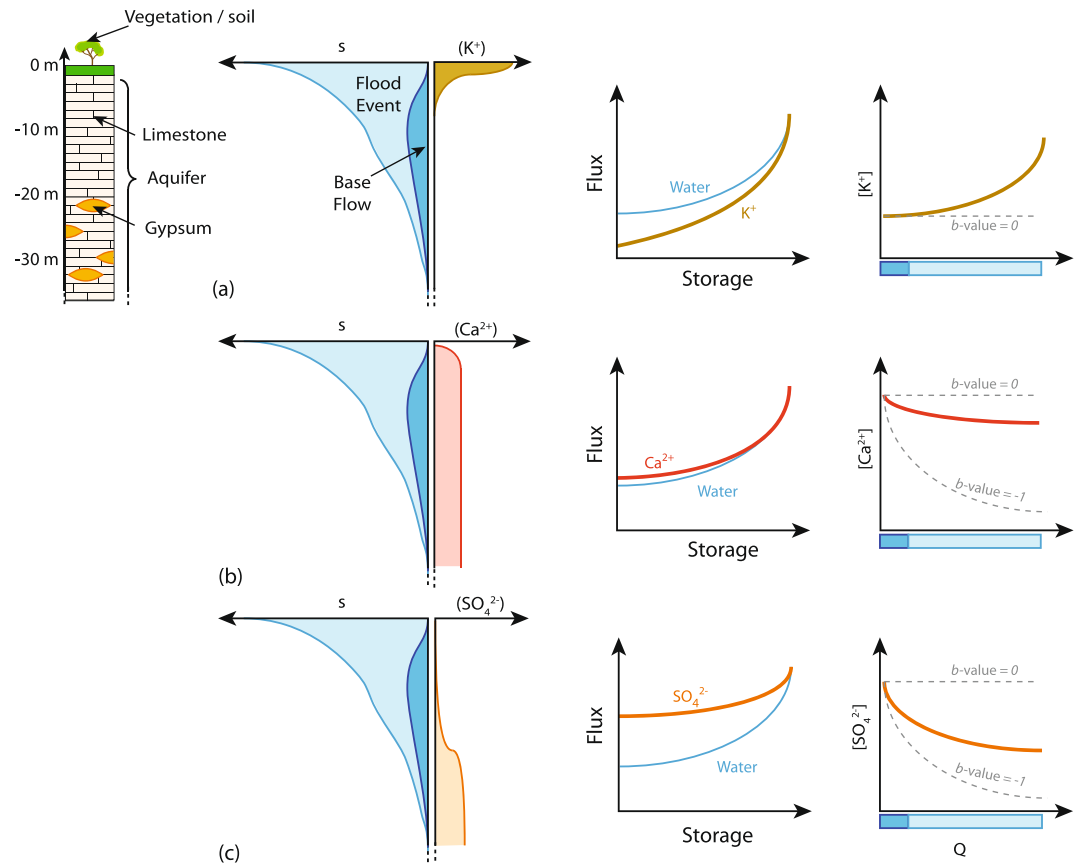


Figure 9. Conceptual representation of the inferred link between water storage s (over base flow in dark blue and over a flood event in light blue) and the solute storage along a “depth-profile” of the Critical Zone at the Orgeval Critical Zone Observatory. Three synthetic cases of vertical distribution of elements throughout the aquifer are presented: (a) enriched at the surface, such as K^+ , by fertilizer inputs and bio-cycling; (b) homogeneously distributed, such as Ca^{2+} , supplied by carbonate dissolution throughout the subsurface; and (c) enriched at the bottom, such as SO_4^{2-} , supplied by the dissolution of gypsum, which occurs deeper below the surface (typically below 20-m depth). For each case, we present a sketch for the expected relationships during the recession period between solute and water flux and storage s (center column), and the corresponding expected $C-Q$ relationship (right column).

depending on the considered solute (Figures 8 and 9; Figure S23 in Supporting Information S1). Hence the hydrological mobility of a solute during floods depends on its chemical properties, and on its spatial distribution and availability in the catchment before the flood occurs. In general, processes forming elemental pools that are readily mobilizable during floods are species-specific, depending on the species distribution within a catchment and on its ability to be delivered to the stream (such as solutes present in isolated or slowly-flowing water bodies, or species adsorbed on mineral and organic surfaces; Herndon et al., 2015). In the particular case of the Orgeval CZO, fertilizers and rain inputs mainly supply Cl^- ; K^+ is supplied by fertilizers and is strongly cycled by vegetation; Ca^{2+} and Mg^{2+} are supplied by carbonate dissolution; and SO_4^{2-} by gypsum dissolution (Floury et al., 2018). All these sources are heterogeneously distributed throughout the Critical Zone of the Orgeval CZO. For example, gypsum lenses are located fairly deep below the surface, whereas fertilizers are spread at the surface. Consequently, our results agree with prior work (Section 1) proposing vertical distributions of these element sources within the Critical Zone as a means of modulating the response to floods, and the way this response changes with antecedent conditions.

As an illustration of how such vertical distributions of elements in the Critical Zone can shape the $C-s$ and corresponding recession $C-Q$ relationships, we present a conceptual sketch for three different types of response of solute export to floods (Figure 9). Our fundamental assumption here is that there exists a close relationship between the water storage and mobilizable elemental pools during a given recession, as discussed above in Section 5.2.2. The three corresponding synthetic cases of vertical distribution of elements throughout the

aquifer are then: (a) enrichment at the surface, for elements such as K^+ added by fertilizer inputs and influenced by bio-cycling; (b) homogenous distributions, where the best example for this scenario at the Orgeval CZO is offered by Ca^{2+} , which at first order is supplied by carbonate dissolution throughout the aquifer; and (c) enrichment at the bottom. An example for the latter behavior at the Orgeval CZO may be offered by SO_4^{2-} , supplied by the dissolution of gypsum, which occurs relatively deep below the surface (Floury et al., 2018). We acknowledge that “in-stream” processes such as those occurring in the hyporheic zone (Burns, 1998; Cohen et al., 2013) are not taken into account in our simplistic concept, although they might affect solute fluxes and their relation to hydrology. Importantly, the simple conceptual interpretation of Figure 9 allows for the production of a diversity of $C-Q$ relationships, even though the water discharge - storage function remains the same for all elements.

6. Conclusion

High-frequency measurements (every 40 min) of major stream solutes (Na^+ , K^+ , Mg^{2+} , Ca^{2+} , Cl^- , SO_4^{2-} , and NO_3^-) at the Orgeval CZO, France, enabled by an example of a “lab-in-the-field” approach called the River Lab, allow for a detailed examination of solute concentration-discharge ($C-Q$) relationships of five major flood events over a hydrologic year. Flood recession $C-Q$ relationships appear to be (a) species-specific with particularly erratic behaviors for K^+ and NO_3^- (most likely linked to the specific timing of fertilizer inputs) whereas more reproducible patterns are observed for Na^+ , Mg^{2+} , Ca^{2+} , Cl^- , and SO_4^{2-} ; (b) event-specific, with a strong dependence on antecedent hydrological conditions, in particular to the level of the shallow aquifer contributing most water to the stream during the recovery period of floods.

The existence of $C-Q$ loops, combined with the fact that recession periods last for much longer than hydrograph rising limbs, suggest that the goodness of a single fit $C-Q$ relationship over a given flood by any mathematical function (be it empirical or derived from a physical theory) will be strongly driven by the recession data alone. In addition, the observed systematic variations between small and intense flood events suggest that the goodness of fit of any mathematical function to a $C-Q$ relationship will be strongly influenced by the most intense floods. Therefore, our observations have important practical implications for the way researchers should use and examine $C-Q$ relationship data sets, depending on the scientific question posed. In particular, the exports of solutes during relatively wet periods of elevated water storage and/or large rain events are fundamentally distinct from those associated with smaller events and dry periods. As a consequence, load estimates focused on event-based solute export should consider such seasonality, and avoid relying on long-term average $C-Q$ patterns (Wang et al., 2024).

Building on the premise that variations in stream solute export during floods are mostly driven by the mobilization of pre-existing water and solute pools within the catchment rather than by shifts in chemical reactivity, we propose a novel framework to consider $C-Q$ response of catchments during floods by recasting in $C-s$ space. With this approach, we are able to propose species-specific models for the response of solute export to changes in water storage in the aquifer of the Orgeval CZO, which is in turn linked to the spatial (in particular vertical) distribution of a given solute throughout the catchment. This study also shows how groundwater level and chemistry data can facilitate testing of hypotheses regarding how the storage of water and elements in a catchment exerts control over $C-Q$ patterns in streams.

In the future, further deployment of similar “lab-in-the-field” devices at other CZOs should allow for a better understanding of the response of solute export to flood events, and shed light on how different chemical pools can contribute to this export. More generally, our work shows how high-frequency measurements of stream chemistry can be used for “auscultating” the Critical Zone.

Data Availability Statement

All River Lab data used in this study are available in Ansart et al. (2020) and via the website: <https://bdoh.irstea.fr/ORACLE/>.

Acknowledgments

We would like to thank Marie Albenque for help with mathematical derivations; Marie Küßner and Jean Marçais for useful comments on an early version of this manuscript, as well as Dan Ibarra and all anonymous reviewers for their comments through the evaluation process.

References

Ackerer, J., Steefel, C., Liu, F., Bart, R., Safeeq, M., O'Geen, A., et al. (2020). Determining how critical zone structure constrains hydrogeochemical behavior of watersheds: Learning from an elevation gradient in California's Sierra Nevada. *Frontiers in Water*, 2, 23. <https://doi.org/10.3389/frwa.2020.00023>

Ansart, P., Azougui, A., Blanchouin, A., Cordier, L., Flourey, P., Gaillardet, J., et al. (2020). High-frequency acquisition of stream chemical data on ORACLE observatory [Dataset]. Recherche Data Gouv, V3. <https://doi.org/10.15454/9PUYPN>

Arora, B., Burrus, M., Newcomer, M., Steefel, C. I., Carroll, R. W. H., Dwivedi, D., et al. (2020). Differential C-Q analysis: A new approach to inferring lateral transport and hydrologic transients within multiple reaches of a mountainous headwater catchment. *Frontiers in Water*, 2, 24. <https://doi.org/10.3389/frwa.2020.00024>

Baronas, J. J., Torres, M. A., Clark, K. E., & West, A. J. (2017). Mixing as a driver of temporal variations in river hydrochemistry: 2. Major and trace element concentration dynamics in the Andes Amazon transition. *Water Resources Research*, 53(4), 3120–3145. <https://doi.org/10.1002/2016wr019729>

Basu, N. B., Destouni, G., Jawitz, J. W., Thompson, S. E., Loukinova, N. V., Darracq, A., et al. (2010). Nutrient loads exported from managed catchments reveal emergent biogeochemical stationarity. *Geophysical Research Letters*, 37(23), L23404. <https://doi.org/10.1029/2010gl045168>

Basu, N. B., Thompson, S. E., & Rao, P. S. C. (2011). Hydrologic and biogeochemical functioning of intensively managed catchments: A synthesis of top-down analyses. *Water Resources Research*, 47(10), W00J15. <https://doi.org/10.1029/2011wr010800>

Benettin, P., Bailey, S. W., Rinaldo, A., Likens, G. E., McGuire, K. J., & Botter, G. (2017). Young runoff fractions control streamwater age and solute concentration dynamics. *Hydrological Processes*, 31(16), 2982–2986. <https://doi.org/10.1002/hyp.11243>

Benettin, P., Rodriguez, N. B., Sprenger, M., Kim, M., Klaus, J., Harman, C. J., et al. (2022). Transit time estimation in catchments: Recent developments and future directions. *Water Resources Research*, 58(11), e2022WR033096. <https://doi.org/10.1029/2022wr033096>

Benettin, P., Soulsby, C., Birkel, C., Tetzlaff, D., Botter, G., & Rinaldo, A. (2017). Using SAS functions and high resolution isotope data to unravel travel time distributions in headwater catchments. *Water Resources Research*, 53(3), 1864–1878. <https://doi.org/10.1002/2016wr020117>

Berner, R. A. (1978). Rate control of mineral dissolution under earth surface conditions. *American Journal of Science*, 278(9), 1235–1252. <https://doi.org/10.2475/ajs.278.9.1235>

Bierzoa, M. Z., Heathwaite, A. L., Bechmann, M., Kyllmar, K., & Jordan, P. (2018). The concentration-discharge slope as a tool for water quality management. *Science of the Total Environment*, 630, 738–749. <https://doi.org/10.1016/j.scitotenv.2018.02.256>

Botter, G., Bertuzzo, E., & Rinaldo, A. (2011). Catchment residence and travel time distributions: The master equation. *Geophysical Research Letters*, 38(11), L11403. <https://doi.org/10.1029/2011gl047666>

Bouchez, J., Espinoza, J. C., Guyot, J., Lagane, C., Filizola, N., Noriega, L., et al. (2017). River mixing in the Amazon as a driver of concentration-discharge relationships. *Water Resources Research*, 53(11), 8660–8685. <https://doi.org/10.1002/2017WR020591>

Boyer, E. W., Hornberger, G. M., Bencala, K. E., & McKnight, D. (1996). Overview of a simple model describing variation of dissolved organic carbon in an upland catchment. *Ecological Modelling*, 86(2–3), 183–188. [https://doi.org/10.1016/0304-3800\(95\)00049-6](https://doi.org/10.1016/0304-3800(95)00049-6)

Brantley, S. L., Holleran, M. E., Jin, L., & Bazilevskaia, E. (2013). Probing deep weathering in the Shale Hills Critical Zone Observatory, Pennsylvania (USA): The hypothesis of nested chemical reaction fronts in the subsurface. *Earth Surface Processes and Landforms*, 38(11), 1280–1298. <https://doi.org/10.1002/esp.3415>

Brutsaert, W., & Nieber, J. L. (1977). Regionalized drought flow hydrographs from a mature glaciated plateau. *Water Resources Research*, 13(3), 637–643. <https://doi.org/10.1029/WR013i003p0637>

Burns, D. A. (1998). Retention of NO₃⁻ in an upland stream environment: A mass balance approach. *Biogeochemistry*, 40(1), 73–96. <https://doi.org/10.1023/A:1005916102026>

Calmels, D., Galy, A., Hovius, N., Bickle, M., West, A. J., Chen, M. C., & Chapman, H. (2011). Contribution of deep groundwater to the weathering budget in a rapidly eroding mountain belt, Taiwan. *Earth and Planetary Science Letters*, 303(1–2), 48–58. <https://doi.org/10.1016/j.epsl.2010.12.032>

Carreau, J., Naveau, P., & Sauquet, E. (2009). A statistical rainfall-runoff mixture model with heavy-tailed components. *Water Resources Research*, 45(10), 1–11. <https://doi.org/10.1029/2009WR007880>

Ceola, S., Botter, G., Bertuzzo, E., Porporato, A., Rodriguez-Iturbe, I., & Rinaldo, A. (2010). Comparative study of ecohydrological streamflow probability distributions. *Water Resources Research*, 46(9), W09502. <https://doi.org/10.1029/2010WR009102>

Cerro, I., Antigüedad, I., Srinavasan, R., Sauvage, S., Volk, M., & Sanchez-Perez, J. M. (2014). Simulating land management options to reduce nitrate pollution in an agricultural watershed dominated by an alluvial aquifer. *Journal of Environmental Quality*, 43(1), 67–74. <https://doi.org/10.2134/jeq2011.0393>

Chanat, J. G., Rice, K. C., & Hornberger, G. M. (2002). Consistency of patterns in concentration-discharge plots. *Water Resources Research*, 38(8), 22. <https://doi.org/10.1029/2001wr000971>

Clow, D. W., & Mast, M. A. (2010). Mechanisms for chemostatic behavior in catchments: Implications for CO₂ consumption by mineral weathering. *Chemical Geology*, 269(1–2), 40–51. <https://doi.org/10.1016/j.chemgeo.2009.09.014>

Cohen, M. J., Kurz, M. J., Heffernan, J. B., Martin, J. B., Douglass, R. L., Foster, C. R., & Thomas, R. G. (2013). Diel phosphorus variation and the stoichiometry of ecosystem metabolism in a large spring-fed river. *Ecological Monographs*, 83(2), 155–176. <https://doi.org/10.1890/12-1497.1>

Diamond, J. S., & Cohen, M. J. (2018). Complex patterns of catchment solute-discharge relationships for coastal plain rivers. *Hydrological Processes*, 32(3), 388–401. <https://doi.org/10.1002/hyp.11424>

Dornblaser, M. M., & Striegl, R. G. (2009). Suspended sediment and carbonate transport in the Yukon River Basin, Alaska: Fluxes and potential future responses to climate change. *Water Resources Research*, 45(6), W06411. <https://doi.org/10.1029/2008wr007546>

Druhan, J. L., & Maher, K. (2017). The influence of mixing on stable isotope ratios in porous media: A revised Rayleigh model. *Water Resources Research*, 53(2), 1101–1124. <https://doi.org/10.1002/2016wr019666>

Duan, S., Kaushal, S. S., Groffman, P. M., Band, L. E., & Belt, K. T. (2012). Phosphorus export across an urban to rural gradient in the Chesapeake Bay watershed. *Journal of Geophysical Research*, 117(G1), G01025. <https://doi.org/10.1029/2011jg001782>

Duncan, J. M., Band, L. E., & Groffman, P. M. (2017). Variable nitrate concentration-discharge relationships in a forested watershed. *Hydrological Processes*, 31(9), 1817–1824. <https://doi.org/10.1002/hyp.11136>

Dupas, R., Musolff, A., Jawitz, J. W., Rao, P. S. C., Jäger, C. G., Fleckenstein, J. H., et al. (2017). Carbon and nutrient export regimes from headwater catchments to downstream reaches. *Biogeosciences*, 14(18), 4391–4407. <https://doi.org/10.5194/bg-14-4391-2017>

Evans, C., & Davies, T. D. (1998). Causes of concentration/discharge hysteresis and its potential as a tool for analysis of episode hydrochemistry. *Water Resources Research*, 34(1), 129–137. <https://doi.org/10.1029/97wr01881>

Fazekas, H. M., Wymore, A. S., & McDowell, W. H. (2020). Dissolved organic carbon and nitrate concentration-discharge behavior across scales: Land use, excursions, and misclassification. *Water Resources Research*, 56(8), e2019WR027028. <https://doi.org/10.1029/2019wr027028>

- Flipo, N., Mouhri, A., Labarthe, B., Biancamaria, S., Rivière, A., & Weill, P. (2014). Continental hydrosystem modelling: The concept of nested stream-aquifer interfaces. *Hydrology and Earth System Sciences*, 18(8), 3121–3149. <https://doi.org/10.5194/hess-18-3121>
- Floury, P., Gaillardet, J., Gayer, E., Bouchez, J., Tallec, G., Ansart, P., et al. (2017). The potamochemical symphony: New progresses in the high frequency acquisition of stream chemical data. *Hydrology and Earth System Sciences Discussions*, 21, 6153–6161. <https://doi.org/10.5194/hess-2017-12>
- Floury, P., Gaillardet, J., Tallec, G., Ansart, P., Bouchez, J., & Gorge, C. (2018). Chemical weathering and CO₂ consumption rate in a multilayered-aquifer dominated watershed under intensive farming: The Orgeval Critical Zone Observatory, France. *Hydrological Processes*, 33(2), 195–213. <https://doi.org/10.1002/hyp.13340>
- Fovet, O., Ruiz, L., Hrachowitz, M., Fauchoux, M., & Gascuel-Oudou, C. (2015). Hydrological hysteresis and its value for assessing process consistency in catchment conceptual models. *Hydrology and Earth System Sciences*, 19(1), 105–123. <https://doi.org/10.5194/hess-19-105-2015>
- Gaillardet, J., Braud, I., Hankard, F., Anquetin, S., Bour, O., Dorfliger, N., et al. (2018). OZCAR: The French network of critical zone observatories. *Vadose Zone Journal*, 17(1), 1–24. <https://doi.org/10.2136/vzj2018.04.0067>
- Garnier, J., Anglade, J., Benoit, M., Billen, G., Puech, T., Ramarson, A., et al. (2016). Reconnecting crop and cattle farming to reduce nitrogen losses to river water of an intensive agricultural catchment (Seine basin, France): Past, present and future. *Environmental Science & Policy*, 63, 76–90. <https://doi.org/10.1016/j.envsci.2016.04.019>
- Garnier, J., Billen, G., Vilain, G., Benoit, M., Passy, P., Tallec, G., et al. (2014). Curative vs. preventive management of nitrogen transfers in rural areas: Lessons from the case of the Orgeval watershed (Seine River basin, France). *Journal of Environmental Management*, 144, 125–134. <https://doi.org/10.1016/j.jenvman.2014.04.030>
- Godsey, S. E., Hartmann, J., & Kirchner, J. W. (2019). Catchment chemostasis revisited: Water quality responds differently to variations in weather and climate. *Hydrological Processes*, 33(24), 3056–3069. <https://doi.org/10.1002/hyp.13554>
- Godsey, S. E., Kirchner, J. W., & CLOW, D. W. (2009). Concentration–discharge relationships reflect chemostatic characteristics of US catchments. *Hydrological Processes*, 23(13), 1844–1864. <https://doi.org/10.1002/hyp>
- Hall, F. R. (1970). Dissolved solids-discharge relationships: 1. Mixing models. *Water Resources Research*, 6(3), 845–850. <https://doi.org/10.1029/wr006i003p00845>
- Hall, F. R. (1971). Dissolved solids-discharge relationships: 2. Applications to field data. *Water Resources Research*, 7(3), 591–601. <https://doi.org/10.1029/wr007i003p00591>
- Harman, C. J. (2015). Time-variable transit time distributions and transport: Theory and application to storage-dependent transport of chloride in a watershed. *Water Resources Research*, 51(1), 1–30. <https://doi.org/10.1002/2014wr015707>
- Herndon, E. M., Dere, A. L., Sullivan, P. L., Norris, D., Reynolds, B., & Brantley, S. L. (2015). Landscape heterogeneity drives contrasting concentration–discharge relationships in shale headwater catchments. *Hydrology and Earth System Sciences*, 19(8), 3333–3347. <https://doi.org/10.5194/hess-19-3333-2015>
- Hornberger, G. M., Bencala, K. E., & McKnight, D. M. (1994). Hydrological controls on dissolved organic carbon during snowmelt in the Snake River near Montezuma, Colorado. *Biogeochemistry*, 25(3), 147–165. <https://doi.org/10.1007/bf00024390>
- Hornberger, G. M., Scanlon, T. M., & Raffensperger, J. P. (2001). Modelling transport of dissolved silica in a forested headwater catchment: The effect of hydrological and chemical time scales on hysteresis in the concentration–discharge relationship. *Hydrological Processes*, 15(10), 2029–2038. <https://doi.org/10.1002/hyp.254>
- House, W. A., & Warwick, M. S. (1998). Hysteresis of the solute concentration/discharge relationship in rivers during storms. *Water Research*, 32(8), 2279–2290. [https://doi.org/10.1016/S0043-1354\(97\)00473-9](https://doi.org/10.1016/S0043-1354(97)00473-9)
- Ibarra, D. E., Caves, J. K., Moon, S., Thomas, D. L., Hartmann, J., Chamberlain, C. P., & Maher, K. (2016). Differential weathering of basaltic and granitic catchments from concentration discharge relationships. *Geochimica et Cosmochimica Acta*, 190, 265–293. <https://doi.org/10.1016/j.gca.2016.07.006>
- Johnson, N. M., Likens, G. E., Bormann, F. H., Fisher, D. W., & Pierce, R. S. (1969). A working model for the variation in stream water chemistry at the Hubbard Brook Experimental Forest, New Hampshire. *Water Resources Research*, 5(6), 1353–1363. <https://doi.org/10.1029/wr005i006p01353>
- Kim, H., Dietrich, W. E., Thurnhoffer, B. M., Bishop, J. K., & Fung, I. Y. (2017). Controls on solute concentration-discharge relationships revealed by simultaneous hydrochemistry observations of hillslope runoff and stream flow: The importance of critical zone structure. *Water Resources Research*, 53(2), 1424–1443. <https://doi.org/10.1002/2016wr019722>
- Kirchner, J. W. (2009). Catchments as simple dynamical systems: Catchment characterization, rainfall-runoff modeling, and doing hydrology backward. *Water Resources Research*, 45(2), 1–34. <https://doi.org/10.1029/2008WR006912>
- Knapp, J. L., Freyberg, J. V., Studer, B., Kieviet, L., & Kirchner, J. W. (2020). Concentration-discharge relationships vary among hydrological events, reflecting differences in event characteristics. *Hydrology and Earth System Sciences Discussions*, 7, 1–27.
- Knapp, J. L., Li, L., & Musolf, A. (2022). Hydrologic connectivity and source heterogeneity control concentration-discharge relationships. *Hydrological Processes*, 36(9), e14683. <https://doi.org/10.1002/hyp.14683>
- Koenig, L. E., Shattuck, M. D., Snyder, L. E., Potter, J. D., & McDowell, W. H. (2017). Deconstructing the effects of flow on DOC, nitrate, and major ion interactions using a high-frequency aquatic sensor network. *Water Resources Research*, 53(12), 10655–10673. <https://doi.org/10.1002/2017wr020739>
- Kolbe, T., De Dreuzy, J. R., Abbott, B. W., Aquilina, L., Babey, T., Green, C. T., et al. (2019). Stratification of reactivity determines nitrate removal in groundwater. *Proceedings of the National Academy of Sciences*, 116(7), 2494–2499. <https://doi.org/10.1073/pnas.1816892116>
- Krier, R., Matgen, P., Goergen, K., Pfister, L., Hoffmann, L., Kirchner, J. W., et al. (2012). Inferring catchment precipitation by doing hydrology backward: A test in 24 small and mesoscale catchments in Luxembourg. *Water Resources Research*, 48(10), 1–15. <https://doi.org/10.1029/2011WR010657>
- Langbein, W. B., & Dawdy, D. R. (1964). *Occurrence of dissolved solids in surface waters in the United States* (pp. 115–117). USGS Professional Paper 501-D.
- Lauzon, N., Anctil, F., & Petrinovic, J. (2004). Characterization of soil moisture conditions at temporal scales from a few days to annual. *Hydrological Processes*, 18(17), 3235–3254. <https://doi.org/10.1002/hyp.5656>
- Li, L. (2019). Watershed reactive transport. *Reviews in Mineralogy and Geochemistry*, 85(1), 381–418. <https://doi.org/10.2138/rmg.2018.85.13>
- Li, L., Bao, C., Sullivan, P. L., Brantley, S., Shi, Y., & Duffy, C. (2017). Understanding watershed hydrogeochemistry: 2. Synchronized hydrological and geochemical processes drive stream chemostatic behavior. *Water Resources Research*, 53(3), 2346–2367. <https://doi.org/10.1002/2016wr018935>
- Li, L., Sullivan, P. L., Benettin, P., Cirpka, O. A., Bishop, K., Brantley, S. L., et al. (2021). Toward catchment hydro-biogeochemical theories. *Wiley Interdisciplinary Reviews: Water*, 8(1), e1495. <https://doi.org/10.1002/wat2.1495>

- Maier, K. (2010). The dependence of chemical weathering rates on fluid residence time. *Earth and Planetary Science Letters*, 294(1–2), 101–110. <https://doi.org/10.1016/j.epsl.2010.03.010>
- Maier, K. (2011). The role of fluid residence time and topographic scales in determining chemical fluxes from landscapes. *Earth and Planetary Science Letters*, 312(1–2), 48–58. <https://doi.org/10.1016/j.epsl.2011.09.040>
- Maier, K., & Chamberlain, C. P. (2014). Hydrologic regulation of chemical weathering and the geologic carbon cycle. *Science*, 343(6178), 1502–1504. <https://doi.org/10.1126/science.1250770>
- Maier, K., & Druhan, J. (2014). Relationships between the transit time of water and the fluxes of weathered elements through the critical zone. *Procedia Earth and Planetary Science*, 10, 16–22. <https://doi.org/10.1016/j.proeps.2014.08.004>
- Marçais, J., De Dreuzy, J. R., Ginn, T. R., Rousseau-Gueutin, P., & Leray, S. (2015). Inferring transit time distributions from atmospheric tracer data: Assessment of the predictive capacities of Lumped Parameter Models on a 3D crystalline aquifer model. *Journal of Hydrology*, 525, 619–631. <https://doi.org/10.1016/j.jhydrol.2015.03.055>
- McDonnell, J. (2014). The two water world hypothesis: Ecohydrological separation of water between streams and trees? *WIREs Water*, 1(4), 323–329. <https://doi.org/10.1002/wat2.1027>
- McIntosh, J. C., Schaumberg, C., Perdrial, J., Harpold, A., Vázquez Ortega, A., Rasmussen, C., et al. (2017). Geochemical evolution of the critical zone across variable time scales informs concentration-discharge relationships: Jemez River Basin Critical Zone Observatory. *Water Resources Research*, 53(5), 4169–4196. <https://doi.org/10.1002/2016wr019712>
- Mei, Y., Hornberger, G. M., Kaplan, L. A., Newbold, J. D., & Aufdenkampe, A. K. (2012). Estimation of dissolved organic carbon contribution from hillslope soils to a headwater stream. *Water Resources Research*, 48(9). <https://doi.org/10.1029/2011wr010815>
- Mei, Y., Hornberger, G. M., Kaplan, L. A., Newbold, J. D., & Aufdenkampe, A. K. (2014). The delivery of dissolved organic carbon from a forested hillslope to a headwater stream in southeastern Pennsylvania, USA. *Water Resources Research*, 50(7), 5774–5796. <https://doi.org/10.1002/2014wr015635>
- Minaudo, C., Dupas, R., Gascuel-Odoux, C., Roubeix, V., Danis, P. A., & Moatar, F. (2019). Seasonal and event-based concentration-discharge relationships to identify catchment controls on nutrient export regimes. *Advances in Water Resources*, 131, 103379. <https://doi.org/10.1016/j.advwatres.2019.103379>
- Moatar, F., Abbott, B. W., Minaudo, C., Curie, F., & Pinay, G. (2017). Elemental properties, hydrology, and biology interact to shape concentration discharge curves for carbon, nutrients, sediment, and major ions. *Water Resources Research*, 53(2), 1270–1287. <https://doi.org/10.1002/2016wr019635>
- Moquet, J. S., Guyot, J. L., Crave, A., Viers, J., Filizola, N., Martinez, J. M., et al. (2016). Amazon River dissolved load: Temporal dynamics and annual budget from the Andes to the ocean. *Environmental Science & Pollution Research*, 23(12), 11405–11429. <https://doi.org/10.1007/s11356-015-5503-6>
- Mouhri, A., Flipo, N., Rejiba, F., de Fouquet, C., Bodet, L., Kurtulus, B., et al. (2013). Designing a multi-scale sampling system of stream-aquifer interfaces in a sedimentary basin. *Journal of Hydrology*, 504, 194–206. <https://doi.org/10.1016/j.jhydrol.2013.09.036>
- Musolff, A., Schmidt, C., Selle, B., & Fleckenstein, J. H. (2015). Catchment controls on solute export. *Advances in Water Resources*, 86, 133–146. <https://doi.org/10.1016/j.advwatres.2015.09.026>
- Nathan, R. J., & McMahon, T. A. (1990). Evaluation of automated techniques for base flow and recession analyses. *Water Resources Research*, 26(7), 1465–1473. <https://doi.org/10.1029/wr026i007p01465>
- Neira, J. M. T., Andréassian, V., Tallec, G., & Mouchel, J. M. (2019). Improved mathematical representation of concentration-discharge relationships. *Hydrology and Earth System Sciences Discussions*. <https://doi.org/10.5194/hess-2019-325>
- Park, Y. S., & Engel, B. A. (2014). Use of pollutant load regression models with various sampling frequencies for annual load estimation. *Water*, 6(6), 1685–1697. <https://doi.org/10.3390/w6061685>
- Pasquet, S., Bodet, L., Dhemaied, A., Mouhri, A., Vitale, Q., Rejiba, F., et al. (2015). Detecting different water table levels in a shallow aquifer with combined P-surface and SH-wave surveys: Insights from VP/VS or Poisson's ratios. *Journal of Applied Geophysics*, 113, 38–50. <https://doi.org/10.1016/j.jappgeo.2014.12.005>
- Pinder, G. F., & Jones, J. F. (1969). Determination of the ground-water component of peak discharge from the chemistry of total runoff. *Water Resources Research*, 5(2), 438–445. <https://doi.org/10.1029/wr005i002p00438>
- Pohle, I., Baggaley, N., Palarea-Albaladejo, J., Stutter, M., & Glendell, M. (2021). A framework for assessing concentration-discharge catchment behavior from low-frequency water quality data. *Water Resources Research*, 57(9), e2021WR029692. <https://doi.org/10.1029/2021wr029692>
- Remondi, F., Kirchner, J. W., Burlando, P., & Fatichi, S. (2018). Water flux tracking with a distributed hydrological model to quantify controls on the spatio-temporal variability of transit time distributions. *Water Resources Research*, 54(4), 3081–3099. <https://doi.org/10.1002/2017wr021689>
- Rice, K. C., Chanat, J. G., Hornberger, G. M., & Webb, J. R. (2004). Interpretation of concentration-discharge patterns in acid-neutralizing capacity during storm flow in three small, forested catchments in Shenandoah National Park, Virginia. *Water Resources Research*, 40(5), W05301. <https://doi.org/10.1029/2003wr002709>
- Rinaldo, A., Benettin, P., Harman, C. J., Hrachowitz, M., McGuire, K. J., Van Der Velde, Y., et al. (2015). Storage selection functions: A coherent framework for quantifying how catchments store and release water and solutes. *Water Resources Research*, 51(6), 4840–4847. <https://doi.org/10.1002/2015wr017273>
- Rode, M., Wade, A. J., Cohen, M. J., Hensley, R. T., Bowes, M. J., Kirchner, J. W., et al. (2016). Sensors in the stream: The high-frequency wave of the present. *Environmental Science & Technology*, 50(19), 10297–10307. <https://doi.org/10.1021/acs.est.6b02155>
- Rose, L. A., Karwan, D. L., & Godsey, S. E. (2018). Concentration-discharge relationships describe solute and sediment mobilization, reaction, and transport at event and longer timescales. *Hydrological Processes*, 32(18), 2829–2844. <https://doi.org/10.1002/hyp.13235>
- Rue, G. P., Rock, N. D., Gabor, R. S., Pitlick, J., Tfiay, M., & McKnight, D. M. (2017). Concentration discharge relationships during an extreme event: Contrasting behavior of solutes and changes to chemical quality of dissolved organic material in the Boulder Creek Watershed during the September 2013 flood. *Water Resources Research*, 53(7), 5276–5297. <https://doi.org/10.1002/2016wr019708>
- Runkel, R. L., Crawford, C. G., & Cohn, T. A. (2004). Load Estimator (LOADEST): A FORTRAN program for estimating constituent loads in streams and rivers (No. 4-A5).
- Seibert, J., Grabs, T., Köhler, S., Laudon, H., Winterdahl, M., & Bishop, K. (2009). Linking soil-and stream-water chemistry based on a Riparian flow-concentration integration model. *Hydrology and Earth System Sciences*, 13(12), 2287–2297. <https://doi.org/10.5194/hess-13-2287-2009>
- Shaw, S. B., & Riha, S. J. (2012). Examining individual recession events instead of a data cloud: Using a modified interpretation of dQ/dt-Q streamflow recession in glaciated watersheds to better inform models of low flow. *Journal of Hydrology*, 434–435, 46–54. <https://doi.org/10.1016/j.jhydrol.2012.02.034>
- Sklash, M. G., & Farvolden, R. N. (1979). The role of groundwater in storm runoff. In *Developments in water science* (Vol. 12, pp. 45–65). Elsevier.

- Speir, S. L., Tank, J. L., Bierzoza, M., Mahl, U. H., & Royer, T. V. (2021). Storm size and hydrologic modification influence nitrate mobilization and transport in agricultural watersheds. *Biogeochemistry*, *156*(3), 319–334. <https://doi.org/10.1007/s10533-021-00847-y>
- Stallard, R. F., & Murphy, S. F. (2014). A unified assessment of hydrologic and biogeochemical responses in Research watersheds in eastern Puerto Rico using runoff-concentration relations. *Aquatic Geochemistry*, *20*(2–3), 115–139. <https://doi.org/10.1007/s10498-013-9216-5>
- Stewart, B., Shanley, J. B., Kirchner, J. W., Norris, D., Adler, T., Bristol, C., et al. (2022). Streams as mirrors: Reading subsurface water chemistry from stream chemistry. *Water Resources Research*, *58*(1), e2021WR029931. <https://doi.org/10.1029/2021wr029931>
- Sullivan, P. L., Ma, L., West, N., Jin, L., Karwan, D. L., Noireaux, J., et al. (2016). CZ-tope at Susquehanna Shale Hills CZO: Synthesizing multiple isotope proxies to elucidate Critical Zone processes across timescales in a temperate forested landscape. *Chemical Geology*, *445*, 103–119. <https://doi.org/10.1016/j.chemgeo.2016.05.012>
- Sullivan, P. L., Stops, M. W., Macpherson, G. L., Li, L., Hirmas, D. R., & Dodds, W. K. (2019). How landscape heterogeneity governs stream water concentration-discharge behavior in carbonate terrains (Konza Prairie, USA). *Chemical Geology*, *527*, 118989. <https://doi.org/10.1016/j.chemgeo.2018.12.002>
- Talleg, G., Ansart, P., Guérin, A., Delaigue, O., & Blanchouin, A. (2015). Observatoire Oracle [Dataset]. Irtsea. <https://doi.org/10.17180/obs.oracle>
- Thompson, S. E., Basu, N. B., Lascrain, J., Jr., Aubeneau, A., & Rao, P. S. C. (2011). Relative dominance of hydrologic versus biogeochemical factors on solute export across impact gradients. *Water Resources Research*, *47*(10), W00J05. <https://doi.org/10.1029/2010wr009605>
- Torres, M. A., Baronas, J. J., Clark, K. E., Feakins, S. J., & West, A. J. (2017). Mixing as a driver of temporal variations in river hydrochemistry: 1. Insights from conservative tracers in the Andes-Amazon transition. *Water Resources Research*, *53*(4), 3102–3119. <https://doi.org/10.1002/2016WR019733>
- Torres, M. A., West, A. J., & Clark, K. E. (2015). Geomorphic regime modulates hydrologic control of chemical weathering in the Andes-Amazon. *Geochimica et Cosmochimica Acta*, *166*, 105–128. <https://doi.org/10.1016/j.gca.2015.06.007>
- Vaughan, M. C., Bowden, W. B., Shanley, J. B., Vermilyea, A., Sleeper, R., Gold, A. J., et al. (2017). High-frequency dissolved organic carbon and nitrate measurements reveal differences in storm hysteresis and loading in relation to land cover and seasonality. *Water Resources Research*, *53*(7), 5345–5363. <https://doi.org/10.1002/2017wr020491>
- Vilain, G., Garnier, J., Talleg, G., & Cellier, P. (2010). Effect of slope position and land use on nitrous oxide (N₂O) emissions (Seine Basin, France). *Agricultural and Forest Meteorology*, *150*(9), 1192–1202. <https://doi.org/10.1016/j.agrformet.2010.05.004>
- Vilain, G., Garnier, J., Talleg, G., & Tournebize, J. (2012). Indirect N₂O emissions from shallow groundwater in an agricultural catchment (Seine Basin, France). *Biogeochemistry*, *111*(1–3), 253–271. <https://doi.org/10.1007/s10533-011-9642-7>
- von Freyberg, J., Studer, B., & Kirchner, J. W. (2017). A lab in the field: High-frequency analysis of water quality and stable isotopes in stream-water and precipitation. *Hydrology and Earth System Sciences Discussions*. <https://doi.org/10.5194/hess-2016-585>
- Wang, J., Bouchez, J., Dolant, A., Flourey, P., Stumpf, A. J., Bauer, E., et al. (2024). Sampling frequency, load estimation and the disproportionate effect of storms on solute mass flux in rivers. *Science of the Total Environment*, *906*, 167379. <https://doi.org/10.1016/j.scitotenv.2023.167379>
- White, A. F., & Blum, A. E. (1995). Effects of climate on chemical weathering in watersheds. *Geochimica et Cosmochimica Acta*, *59*(9), 1729–1747. [https://doi.org/10.1016/0016-7037\(95\)00078-E](https://doi.org/10.1016/0016-7037(95)00078-E)
- Winnick, M. J., Carroll, R. W., Williams, K. H., Maxwell, R. M., Dong, W., & Maher, K. (2017). Snowmelt controls on concentration-discharge relationships and the balance of oxidative and acid-base weathering fluxes in an alpine catchment, East River, Colorado. *Water Resources Research*, *53*(3), 2507–2523. <https://doi.org/10.1002/2016wr019724>
- Wittenberg, H. (1999). Baseflow recession and recharge as nonlinear storage processes. *Hydrological Processes*, *13*(5), 715–726. [https://doi.org/10.1002/\(sici\)1099-1085\(19990415\)13:5<715::aid-hyp775>3.0.co;2-n](https://doi.org/10.1002/(sici)1099-1085(19990415)13:5<715::aid-hyp775>3.0.co;2-n)
- Wolock, D. M., Fan, J., & Lawrence, G. B. (1997). Effects of basin size on low flow stream chemistry and subsurface contact time in the Neversink River watershed, New York. *Hydrological Processes*, *11*(9), 1273–1286. [https://doi.org/10.1002/\(sici\)1099-1085\(199707\)11:9<1273::aid-hyp557>3.0.co;2-s](https://doi.org/10.1002/(sici)1099-1085(199707)11:9<1273::aid-hyp557>3.0.co;2-s)
- Wymore, A. S., Brereton, R. L., Ibarra, D. E., Maher, K., & McDowell, W. H. (2017). Critical zone structure controls concentration discharge relationships and solute generation in forested tropical montane watersheds. *Water Resources Research*, *53*(7), 6279–6295. <https://doi.org/10.1002/2016wr020016>
- Wymore, A. S., Larsen, W., Kincaid, D. W., Underwood, K. L., Fazekas, H. M., McDowell, W. H., et al. (2023). Revisiting the origins of the power-law analysis for the assessment of concentration-discharge relationships. *Water Resources Research*, *59*(8), e2023WR034910. <https://doi.org/10.1029/2023wr034910>
- Wymore, A. S., Leon, M. C., Shanley, J. B., & McDowell, W. H. (2019). Hysteretic response of solutes and turbidity at the event scale across forested tropical montane watersheds. *Frontiers in Earth Science*, *7*, 126. <https://doi.org/10.3389/feart.2019.00126>
- Xiao, D., Brantley, S. L., & Li, L. (2021). Vertical connectivity regulates water transit time and chemical weathering at the hillslope scale. *Water Resources Research*, *57*(8), e2020WR029207. <https://doi.org/10.1029/2020wr029207>
- Zhi, W., & Li, L. (2020). The shallow and deep hypothesis: Subsurface vertical chemical contrasts shape nitrate export patterns from different land uses. *Environmental Science & Technology*, *54*(19), 11915–11928. <https://doi.org/10.1021/acs.est.0c01340>
- Zhi, W., Li, L., Dong, W., Brown, W., Kaye, J., Steefel, C., & Williams, K. H. (2019). Distinct source water chemistry shapes contrasting concentration-discharge patterns. *Water Resources Research*, *55*(5), 4233–4251. <https://doi.org/10.1029/2018wr024257>
- Zribi, M., Baghdadi, N., Holah, N., Fafin, O., & Guérin, C. (2005). Evaluation of a rough soil surface description with ASAR-ENVISAT radar data. *Remote Sensing of Environment*, *95*(1), 67–76. <https://doi.org/10.1016/j.rse.2004.11.014>
- Zribi, M., & Dechambre, M. (2003). A new empirical model to retrieve soil moisture and roughness from C-band radar data. *Remote Sensing of Environment*, *84*(1), 42–52. [https://doi.org/10.1016/S0034-4257\(02\)00069](https://doi.org/10.1016/S0034-4257(02)00069)

References From the Supporting Information

- Valluri, S. R., Jeffrey, D. J., & Corless, R. M. (2000). Some applications of the Lambert's W Function to physics. *Canadian Journal of Physics*, *78*(9), 823–831. <https://doi.org/10.1139/p00-065>